Membrane curvature governs the distribution of Piezo1 in live cells

Shilong Yang, Xinwen Miao, Steven Arnold, Boxuan Li, Alan T. Ly, Huan Wang, Matthew Wang, Xiangfu Guo, Medha M. Pathak, Wenting Zhao, Charles D. Cox, Zheng Shi ✉

Department of Chemistry and Chemical Biology, Piscataway, NJ 08854, United States • School of Chemistry, Chemical Engineering, and Biotechnology, Nanyang Technological University, 637457, Singapore • Department of Cell Biology and Neuroscience, Piscataway, NJ 08854, United States • Department of Physiology & Biophysics, UC Irvine, CA 92697, United States • Sue and Bill Gross Stem Cell Research Center • Department of Physics, Rutgers University, Piscataway, NJ 08854, United States • Molecular Cardiology and Biophysics Division, Victor Chang Cardiac Research Institute, Sydney, NSW, Australia • Cancer Pharmacology Research Program, Cancer Institute of New Jersey, Rutgers University, New Brunswick, NJ 08901, United States

Endorsement statement (6 December 2022)

The preprint by Yang *et al*. asks how the shape of the membrane influences the localization of mechanosensitive Piezo channels. The authors use a creative approach involving methods that distort the plasma membrane by generating blebs and artificial filopodia. They convincingly show that curvature of the lipid environment influences Piezo1 localization, such that increased curvature causes channel depletion, and that application of the chemical modulator Yoda1 is sufficient to allow channels to enter filopodia. The study provides support for a provocative "flattening model" of Yoda1 action, and should inspire future studies by researchers interested in mechanosensitive channels and membrane curvature.

(This endorsement by Biophysics Colab refers to version 2 of this preprint, which has been revised in response to peer review of version 1.)

Abstract

Piezo1 is a *bona fide* mechanosensitive ion channel ubiquitously expressed in mammalian cells. The distribution of Piezo1 within a cell is essential for various biological processes including cytokinesis, cell migration, and wound healing. However, the underlying principles that guide the subcellular distribution of Piezo1 remain largely unexplored. Here, we demonstrate that membrane curvature serves as a key regulator of the spatial distribution of Piezo1 in the plasma membrane of living cells. Piezo1 depletes from highly curved membrane protrusions such as filopodia and enriches to nanoscale membrane invaginations. Quantification of the curvaturedependent sorting of Piezo1 directly reveals the *in situ* nano-geometry of the Piezo1-membrane complex. Piezo1 density on filopodia increases upon activation, independent of Ca^{2+}, suggesting flattening of the channel upon opening. Consequently, the expression of Piezo1 inhibits filopodia formation, an effect that diminishes with channel activation.

Introduction

Piezo1 is a widely expressed mechanosensitive ion channel in the plasma membrane of eukaryotic cells[1],[2], crucial for a broad range of mechanotransduction processes[3]–[5]. Each Piezo1 monomer contains 38 transmembrane helices and cryogenic electron microscopy (CryoEM) shows a trimeric propeller-like assembly which is thought to curve into the cytosol in its resting state[6]–[9]. Recently, a flattened configuration of Piezo1 was identified when reconstituted into small liposomes, potentially corresponding to the open/inactivated state of the ion channel[10] and confirming previous work using high speed atomic force microscopy (HS-AFM)[11]. The large size and curved architecture of Piezo1 trimers make them directly sensitive to tension in the plasma membrane[7], [12]–[14]. Additionally, several studies indicate a cytoskeletal role in the activation of Piezo channels, while the presence of direct Piezo1-cytoskeleton interaction is still under debate[15]–[22]. Notably, the cortical cytoskeleton can drastically affect the extent of membrane tension propagation, thereby indirectly controlling Piezo1 activation via the lipid bilayer[23]–[26].

While the structure and activation of individual Piezo1 channels have been extensively studied, the dynamics and distribution of the channel within a cell are only starting to be explored[19],[21],[25],[27]. In addition, it is unclear whether the Piezo1 structures determined *in vitro* recapitulate its nanoscale conformations in living cells[7], [8],[10],[11]. Several recent studies highlighted a preferential subcellular distribution of Piezo1: First, a polarized distribution of Piezo1 towards the rear of migrating keratinocytes plays a crucial role in controlling the speed of wound healing[28]. Additionally, Piezo1 has been found to enrich at subcellular structures that are important for mechanotransduction, such as focal adhesion sites[27], [29] and T-tubules of cardiomyocytes[30],[31]. Lastly, Piezo1 has been reported to preferentially localize to the intercellular bridge during cytokinesis[32], and to the biconcave 'dimples' in red blood cells[19],[21]. While a general mechanistic explanation has yet to be established, these intriguing subcellular patterns of Piezo1 raise the question of whether this ion channel can be sorted by fundamental physical factors on the cell surface.

Several hints in the literature indicate that membrane curvature may play a role in regulating the cellular distribution of Piezo1. First, the structure of purified Piezo1 trimers shows that they form nanoscale invaginations in a simple liposomal system[7], [11]. When locally stretching membrane tethers to activate Piezo1, Ca^{2+} influx initiates around the tether-cell attachment point where membrane tension is high[23]. However, Ca^{2+} initiation sites are noticeably missing from the highly tensed membrane tether itself[23]. More surprisingly, a recent study showed that force dependent Ca^{2+} signals in filopodia are independent of Piezo channels[33]. Filopodia are highly curved membrane protrusions that geometrically resemble the artificially pulled membrane tethers (tube of radius ~ 50 nm). Thus, a simple explanation would be that Piezo1 are actually absent from these highly curved membrane protrusions.

Here, we combine high-throughput filopodia[34] and nanobar[35],[36] sorting assays with quantitative single membrane tether pulling experiments[23] to show that membrane curvature is a fundamental regulator of Piezo1's distribution within the plasma membrane. The curvature mismatch between Piezo1 and membrane protrusions prevents the channel from entering structures such as filopodia and thin membrane tethers. In contrast, Piezo1 significantly enriches to curved cell membrane invaginations induced by engineered nanobars[35],[36]. Quantifying the curvature preference of Piezo1 on a wide range of tether radii reveals the nano-geometry of Piezo1-membrane complex in living cells. Furthermore, a chemical activator of Piezo1, Yoda1, which has been hypothesized to serve as a molecular wedge to bias the protein towards a less-curved state[37], allows Piezo1 to enter filopodia in a Ca^{2+}-independent manner. The curvaturepreference and Yoda1-response of Piezo1 sorting in cells are consistent with recently determined structural features of purified Piezo1 trimers[10]. The coupling between curvature

dependent sorting and activation of Piezo1 in living cells likely represents a fundamental cornerstone of Piezo1 channel biology, enabling the regulation of filopodia formation and retaining Piezo1 in the cell body during cell migration.

Results

Piezo1 is depleted from filopodia

To study the distribution of Piezo1 in the plasma membrane, we first co-expressed human Piezo1 (hPiezo1-eGFP[12]) and glycosylphosphatidylinositol (GPI) anchored mCherry in HeLa cells. Piezo1 traffics well to the plasma membrane, as indicated by an eGFP fluorescence profile across the cell body that closely resembles the co-expressed plasma membrane marker (Fig. 1A, Fig. S1). However, the Piezo1 signal was noticeably missing on filopodia that protrudes around the edge of the cell, in drastic contrast with membrane markers such as GPI and CaaX, and with other transmembrane proteins such as the dopamine receptor D2 (D2R) and the mechanosensitive potassium channel TREK1 (Fig. 1A–1C and Fig. S2). To systematically quantify protein densities on filopodia, we defined a unitless filopodia sorting value (S_{filo}) using the fluorescence ratio between the molecule of interest (MOI) and the membrane reference (Fig. S3, Methods). This fluorescence ratio measured along a filopodium is normalized to the same ratio on a flat region of the cell body to account for cell-cell variabilities. Additionally, the well-defined membrane geometry on a flat region of the cell allows us to directly quantify the diffraction-limited radii of filopodia from the fluorescence of membrane markers[23].

We found the S_{filo} of Piezo1 is close to 0, significantly smaller than the sorting of other MOIs (S_{filo} ~ 1; Fig. 1D). The lack of Piezo1 on filopodia is independent of imaging temperature, the choice of fluorescent protein (FP) tag, FP fusion position, or Piezo1 species (Fig. 1D). In addition to HeLa cells, Piezo1 is depleted from the filopodia of HEK293T (Fig. S4) and from the filopodia of mouse embryonic fibroblasts (MEFs) where tdTomato-labelled Piezo1 is expressed at endogenous levels (Fig. S5)[25,28]. Referencing to the endogenous Piezo1-tdTomato fluorescence in MEFs, the amount of overexpressed Piezo1 in HeLa cells is estimated to be 2.5 ± 1.5 (mean ± SD, n = 12) fold (Fig. S5C). Notably, D2R and TREK1 are significantly enriched on filopodia (S_{filo} > 1). The filopodia enrichment of D2R agrees with established membrane curvature preference of GPCRs[34], whereas the enrichment of TREK1 potentially reflects the protein's role in filopodia formation[38]. Cells that overexpress Piezo1 had the same filopodia radii as cells expressing membrane markers (Fig. 1E). In contrast, cells overexpressing D2R or TREK1 showed significantly reduced filopodia radii, consistent with the membrane deformation and curvature generation ability of many curvature sensing proteins[39,40]. However, the molecular mechanisms and the causalities between the increased S_{filo} and the reduced filopodia radii in D2R or TREK1 expressing cells remain to be explored.

The absence of Piezo1 on filopodia is consistent with the dispensability of Piezo1 for mechanically activated Ca^{2+} signals in filopodia[33]. Additionally, the quantified curvature preference of Piezo1 (S_{filo} = 0.027 ± 0.003, mean ± SEM) is in accord with a recent CryoEM observation that only ~3% of purified Piezo1 trimers were oriented 'outside-out' (extracellular domains of Piezo1 facing the outside of liposomes), as a Piezo1 trimer on filopodia would be, when reconstituted into highly curved liposomes[10].

Depletion of Piezo1 is not specific to filopodia and is independent of cytoskeleton

Cellular protrusions such as filopodia typically contain a complex network of actin-rich structures[41]. Is the observed depletion of Piezo1 in Fig. 1 specific to filopodia? To answer this question, we focused our further investigation on membrane tethers that geometrically mimic
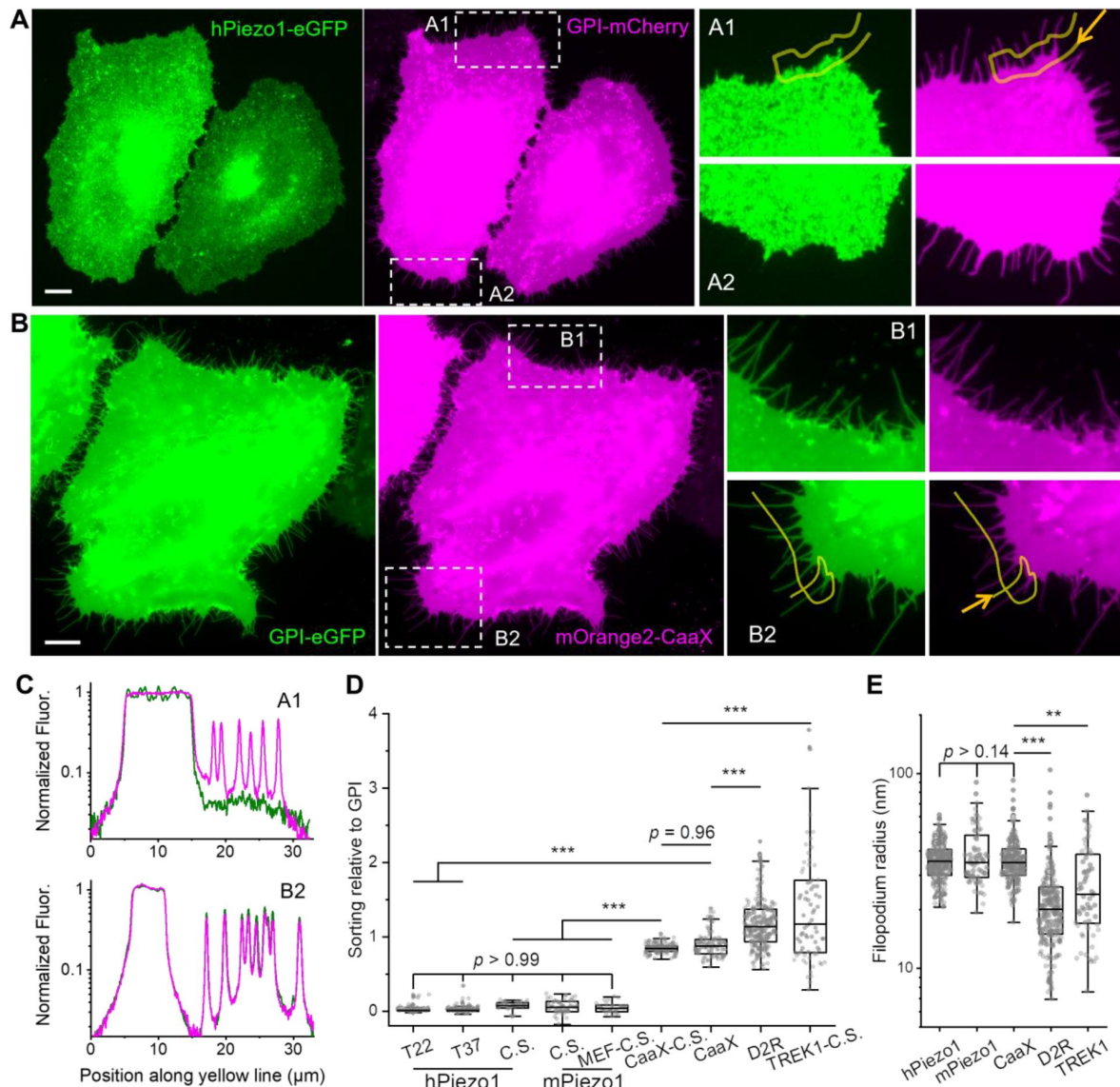
Figure 1.

Piezo1 is depleted from filopodia.

(A) Fluorescence images of HeLa cells co-expressing hPiezo1-eGFP (left) and GPI-mCherry (middle). The two boxed regions (A1, A2) are zoomed-in on the right. Images are contrast-adjusted to show the dim filopodia, see Fig. S1A for images under regular contrast. **(B)** Fluorescence images of HeLa cells co-expressing GPI-eGFP (left) and mOrange2-CaaX (middle). The two boxed regions (B1, B2) are zoomed-in on the right. All scale bars are 10 μm. **(C)** Fluorescence intensity profiles along the marked yellow lines in A1 (up) and B2 (down). Green: hPiezo1 (up) and GPI (down). Magenta: GPI (up) and CaaX (down). Each fluorescence trace was normalized to the mean intensity on the corresponding flat cell body. **(D)** Filopodia sorting of eGFP fused hPiezo1 (T22: at 22°C, n.f. = 129, n.c. = 12; T37: at 37°C, n.f. = 113, n.c. = 8), CaaX (n.f. = 87, n.c. = 9), and D2R (n.f. = 222, n.c. = 15) relative to GPI-mCherry. C.S.: color swap, indicating the molecule of interest was fused with red or orange fluorescent proteins (tdTomato for MEF, mOrange2 for CaaX, mCherry for the rest) while the reference was GPI-eGFP. hPiezo1-C.S.: n.f. = 24, n.c. = 4; mPiezo1-C.S.: n.f. = 47, n.c. = 8; mPiezo1-MEF-C.S.: n.f. = 24, n.c. = 5; CaaX-C.S.: n.f. = 123, n.c. = 9; TREK1-C.S.: n.f. = 77, n.c. = 12. n.f.: number of filopodia, n.c.: number of cells. **(E)** Filopodia radii of cells co-expressing GPI and hPiezo1 (n.f. = 266), mPiezo1 (n.f. = 71), CaaX (n.f. = 210), D2R (n.f. = 222), or TREK1 (n.f. = 65). All radii were determined from the GPI channel. Data labelled with 'MEF' were done in mouse embryonic fibroblasts with Piezo1-tdTomato at endogenous expression level and 'TREK1' were measured in HEK293T cells due to TREK1's poor expression in HeLa cells, all other quantifications were done in HeLa cells. In the box (25% ~ 75%) plots, the mid-lines represent the median and the whiskers represent the 1.5 inter-quartile range (same below). p values given by one-way ANOVA with *post hoc* Tukey's test. ***$p < 10^{-7}$. **$p < 10^{-3}$.

filopodia but lack specific actin-based structures when freshly pulled[23] (Fig. 2A).

Similar to the observation on filopodia, tethers pulled from HeLa cells or MEFs only contained signal for the membrane marker (Fig. 2B, Fig. S5B), and no significant difference could be found between Piezo1's sorting on tethers (S_{teth}) and on filopodia (S_{filo}) (Fig. 2E). The geometrical similarity between tethers and filopodia (both are highly curved membrane protrusions) points to a possible role of membrane curvature in mediating the sorting of Piezo1. However, S_{filo} did not show any apparent dependence on filopodium radius, unlike that of D2R or TREK1 (Fig. S6). Additionally, S_{teth} is independent of the relaxation of pulled tethers (Fig. S7). Notably, filopodia only present a small range of membrane radii (25 ~ 50 nm). Radii of short and fully relaxed tethers are similar to those of filopodia, while stretched tethers are typically thinner[23] (Fig. 2F). Therefore, we hypothesize that the sorting of Piezo1 is most sensitive to membrane curvatures corresponding to > 50 nm radii protrusions. Alternatively, it is plausible that Piezo1 is strongly attached to the cortical cytoskeleton, preventing the channel from moving onto membrane protrusions.

To test the two hypotheses, we generated stable membrane blebs via pharmacological depolymerization of the actin cytoskeleton[23]. Similar to previous reports[12], bleb membranes clearly contain Piezo1 signal, but not significantly enriched relative to the cell body (Fig. 2C, 2D; Fig. S8). More importantly, negligible Piezo1 fluorescence was observed on membrane tethers pulled from tense blebs (Fig. 2C). Plasma membrane blebs do not contain cytoskeleton, therefore results such as Fig. 2C directly argue against a main cytoskeletal role in the depletion of Piezo1 from tethers. The radius of a tether pulled from the bleb is determined by the bleb's membrane tension[23], which is in turn governed by the intracellular pressure[42]. We found that membrane blebs triggered by actin depolymerization exhibited a wide range of apparent 'floppiness', likely a result of stochastic pressure release during bleb formation. On floppy (i.e., low membrane tension) blebs, pulled tethers showed much wider apparent radii (Fig. 2D; eq. S6). Importantly, Piezo1 fluorescence can be clearly observed on these wide tethers, leading to a highly scattered S_{teth} of Piezo1 on tethers pulled from blebs (Fig. 2E). Tethers are typically imaged > 1 min after pulling, whereas membrane tension equilibrates within 1 s across cellular scale free membranes (e.g., bleb, tether)[23]. Therefore, the sorting of Piezo1 within individual tension-equilibrated tether-bleb systems (Fig. 2C – 2G) suggests that membrane curvature can directly modulate Piezo1 distribution beyond potential confounding tension effects.

When combining the Piezo1 sorting and the tether radius measurements together, a clear positive correlation can be observed, with S_{teth} on tense blebs comparable to S_{teth} measured on intact cells and to the fraction of 'outside-out' Piezo1 trimers when reconstituted into small liposomes[10] (Fig. 2G). S_{teth} of Piezo1 is independent of bleb radius (Fig. 2G, inset), confirming the lack of optical artifacts induced by bleb curvature. However, the curved geometry of blebs only allowed determination of an apparent tether radius (Fig. S3). We assumed that the average radius of filopodia and equilibrated tethers from cell body are equal to the radii of tethers from the tensest blebs, thus converting the apparent radii (in A.U.) to absolute radii (in nm) of tethers from blebs (Fig. 2F, 2G). The conversion was consistent with the upper bound of tether diameters set by the width of optically resolvable catenoid-shape membranes at the two ends of low-tension tethers[43] (Fig. S8C).

Quantification of Piezo1's molecular features

The trimer of Piezo1 has been suggested to adopt an 'outside-in' dome shape in liposomal systems[7,10,11,44]. If this were to occur in cells, Piezo1 would energetically prefer certain membrane invaginations (positive curvature) and stay away from membrane protrusions
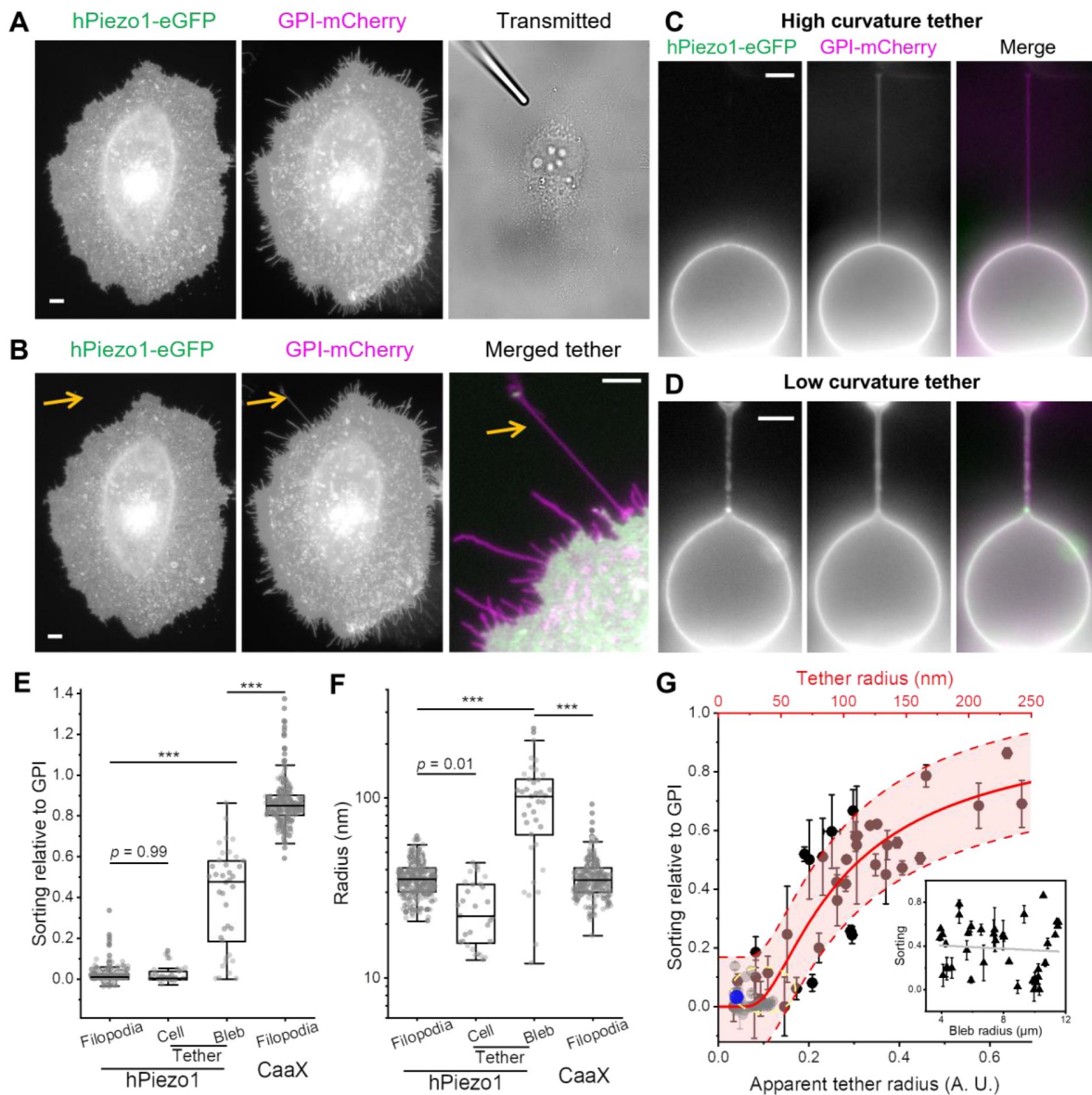
Figure 2.

Sorting of Piezo1 on membrane tethers.

(A) Fluorescence images of a HeLa cell co-expressing hPiezo1-eGFP (left) and GPI-mCherry (middle). The transmitted light image (right) shows the position of a motorized micropipette (fused-tip) in contact with the cell before tether pulling. **(B)** Fluorescence images of the HeLa cell in (**A**) after a 20 µm tether was pulled out (arrow). The tether region is merged and contrast-adjusted on the right. **(C, D)** Fluorescence images of tethers pulled from membrane blebs on HeLa cells co-expressing hPiezo1-eGFP (left) and GPI-mCherry (middle). Merged images shown on the right. Significantly less Piezo1 signals were observed on the tether from tense bleb (**C**) compared to the tether from floppy bleb (**D**). All fluorescence images here are shown in log-scale to highlight the dim tether. All scale bars are 5 µm. Full images of the cell in (**C**) and (**D**) are shown in Fig. S8. **(E, F)** Sorting of hPiezo1 (**E**) and radii of tethers (**F**) pulled from cell membranes (Cell, n = 31 cells) and membrane blebs (Bleb, n = 38 blebs) relative to GPI. Corresponding data of hPiezo1 (n = 266 filopodia) and CaaX (n = 210 filopodia) from Fig. 1D ⤴ and Fig. 1E ⤴ are shown here for comparison. All radii were determined from the GPI channel. **(G)** Sorting of hPiezo1 on tethers pulled from blebs (black) plotted as a function of the apparent (lower axis) and absolute (upper axis) radii of the tethers. Sorting of hPiezo1 on tethers pulled from cells are shown in gray. The fraction of 'outside-out' Piezo1 when reconstituted into small liposomes (according to ref[10]) is shown in blue. The yellow circle shows the cluster of tense bleb data used to calculate the conversion factor for tether radius. The solid line is a two-parameter fit (R^2 ⤴ = 0.85, n = 69 tethers) with the shaded area representing the 95% confidence interval. Inset: Sorting of Piezo1 as a function of bleb radius (n = 38 blebs), where the line represents a linear fit with slope = −0.007 ± 0.015 µm⁻¹. Error bars are SEM. *p* values given by one-way ANOVA with *post hoc* Tukey's test. ***$p < 10^{-7}$.

(negative curvature) such as the filopodium and tether. Accordingly, we fitted our measured relation between the sorting of Piezo1 on tether (S_t) and the tether radius (R_t) in Fig. 2G � to a 2-parameter model based on the bending energy of membrane protrusions (Method)[34]�, [45]�:

$$S_t = \exp\left[-\widetilde{A_P}\left(\frac{1}{R_t^2} + \frac{2C_0}{R_t}\right)\right] \quad (1)$$

Here $\widetilde{A_P} = \frac{\tilde{\kappa}A_P}{2k_B T}$ is the product of the unit area for each Piezo1-membrane complex (A_p) and its bending stiffness ($\tilde{\kappa}$), normalized by the Boltzmann constant (k_B) and the absolute temperature (T). A_p represents the area of a potentially curved surface and should not be confused with the projected area of the protein. C_0, expected to be positive for Piezo1, is the spontaneous curvature of each protein-membrane complex in the (mostly flat) plasma membrane and would be lower than the apparent curvature of Piezo1 in detergents or in highly curved liposomes[10]�,[11]�, [44]�.

The two fitting parameters $\widetilde{A_P}$ and C_0 correspond to the contributions of Piezo1's size (larger proteins have a stronger tendency to stay away from highly curved membranes) and intrinsic curvature, respectively. The fitting gave $\widetilde{A_P}$ = 2400 ± 1000 nm² and C_0^{-1} = 83 ± 17 nm. The spontaneous curvature of the Piezo1-membrane complex C_0 represents a balance between the intrinsic curvature of Piezo1 trimers (0.04 ~ 0.2 nm^{-1} as suggested by CryoEM studies[10]�,[11]�, [44]�) and that of the associated membrane (0 nm^{-1}, assuming lipid bilayers alone do not have an intrinsic curvature and the formation of tether is only due to the external pulling force), consistent with the large amount of lipids associated with the dome of the propeller-shaped Piezo1 trimers[7]�, [10]�. Combining tether pulling force and tether radius measurements[23]�, the resulted membrane bending stiffness of Piezo1-expressing HeLa cells was 13.6 ± 3.8 k_BT (n = 9), comparable to that of HeLa cell blebs: 12.7 ± 2.5 k_BT (n = 14; Fig. S9). The similarity between the bending stiffnesses of cell and bleb membranes suggest minimal compositional change during bleb formation[46]�. Using the bending stiffness of bleb membranes, we estimated the area of each Piezo1 unit A_P = 380 ± 170 nm^2�, in agreement with the area of Piezo1 trimers measured with CryoEM (~ 400 nm^2�)[10]�, [11]�, [14]�, [44]�

Enrichment of Piezo1 on membrane invaginations

While the previous measurements focus on the behavior of Piezo1 on membrane protrusions, the model can be directly extended to estimate the sorting of Piezo1 on membrane invaginations. It is worth noting that contributions from the size and the spontaneous curvature of Piezo1 are synergistic in the case of protrusions (eq. S14�) but can cancel each other out on invaginations (eq. S15�). Therefore, the enrichment of Piezo1 onto invaginations is predicted to be much less prominent than the depletion of Piezo1 from protrusions, with the sorting of Piezo1 peaking at 1.41 when the radius of invagination is 83 nm (Fig. S10, Methods). Moreover, the enrichment of Piezo1 is predicted to be only (7 ± 35) % on 25 ~ 75 nm invaginations compared to an (87 ± 10) % depletion effect on protrusions of the same range of radii. This is consistent with the lack of obvious Piezo1 enrichment spots in the bulk of the plasma membrane where highly curved (< 50 nm radius) invaginations such as endocytic sites and caveolae are expected (Fig. S1-S5).

To explore potential enrichment of Piezo1 on membrane invaginations, we grew hPiezo1-expressing cells on substrates that have been finely engineered with nanobars[35]�, [36]�. Each nanobar presents two curved ends and a flat central region (Fig. 3A�) and can be duplicated with high precision (Fig. 3B�). When cells are cultured on top of nanobar-patterned substrates, their basal membranes will adapt to the geometry of the substrate and form membrane invaginations in parallel[36]�. In hPiezo1-eGFP expressing cells, Piezo1 tends to enrich towards the curved ends, whereas the membrane marker (CellMask Deep Red) homogeneously distributes across the entire nanobar (Fig. 3C�). By averaging over hundreds of nanobars with 3 different diffractionlimited widths (200, 300, 400 nm), we observed clear enrichments of Piezo1 towards the curved ends as compared to the flat central regions of nanobars (Fig. 3D�, 3E�). For all three nanobar widths, the end-to-center ratios for Piezo1 are significantly higher than those for the membrane marker

(Fig. 3E ⧉, 3F ⧉). The median of Piezo1's enrichment at the curved ends (relative to the membrane marker) ranges from 1.31 to 1.49, comparable to the predicted sorting of Piezo1 in this range of membrane curvature (Fig. S10; S = 1.26 ~ 1.40 for invagination radius of 100 ~ 200 nm) and to established sensors for membrane invaginations[47] ⧉. The sorting of Piezo1 was not significantly different between the three nanobar widths (Fig. 3F ⧉), consistent with the predicted low curvature sensitivity on 100 ~ 200 nm invaginations ($|\mathrm{d}S/\mathrm{d}R|$ < 2 µm^{-1}, which is more than 4-fold lower than $|\mathrm{d}S/\mathrm{d}R|$ around 55 nm protrusions; Fig. S10). While further investigations on a wider range of membrane curvature are required to fully map out the sorting of Piezo1 on membrane invaginations, our data (Fig. 3 ⧉) clearly suggest that membrane curvature can lead to enrichment of Piezo1 on cellular invaginations.

Yoda1 leads to a Ca^{2+} independent increase of Piezo1 on tethers

Yoda1 is a Piezo1 agonist that has been hypothesized to bias the channel towards a less-curved state[37] ⧉. Equation (1) ⧉ predicts that a smaller C_0 would lead to an increase of Piezo1 density on protrusions (Fig. S10). Indeed, a significantly increased amount of Piezo1 signal was observed on filopodia after adding 10 µM of Yoda1, while the radii of these filopodia remain unaltered (Fig. 4A-C ⧉, S11A). Additionally, the S_{filo} of activated Piezo1 showed a positive correlation with filopodia radii (Fig. 3D ⧉; Pearson's r = 0.59). Assuming the size of Piezo1 doesn't change during activation ($\widetilde{A_P}$ = 2400 nm²), our model predicts a spontaneous curvature $C_0{}^{-1}$= (4 ± 13) µm of the Piezo1-membrane complex in the presence of Yoda1, corresponding to an essentially flat geometry (Fig. 4D ⧉, S10). The Yoda1 effect on Piezo1 sorting was not instantaneous, taking more than 5 min to equilibrate (Fig. S12A). This is consistent with the measured mean diffusion coefficient of Piezo1 on the cell membrane (Fig. S12B; 0.0021± 0.0004 µm² ⧉/s, n = 44), indicating that Piezo1 trimers diffuse from the cell body to filopodia after Yoda1-induced activation.
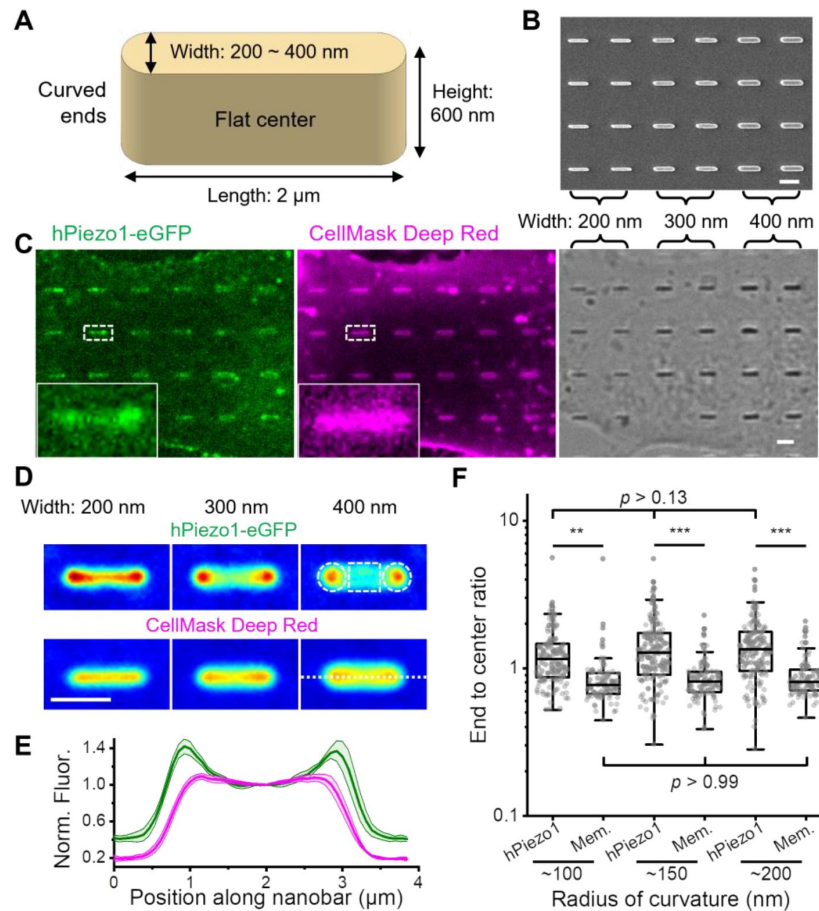
Figure 3.

Enrichment of Piezo1 towards the ends of nanobars.

(A) Illustration of a nanobar. (B)l Scanning electron microscopy image of the cell culture substrate with 200, 300, and 400 nm wide nanobars. (C) A representative image of cells cultured on nanobar substrate, expressing hPiezo1-eGFP (left) and stained with CellMask Deep Red (middle). The transmitted light image is shown on the right with the width of nanobars labelled on top. (D) Averaged fluorescence images (up: hPiezo1; down: CellMask Deep Red) of nanobars with widths of 200 nm (left; n = 141 nanobars); 300 nm (middle; n = 167 nanobars); 400 nm (right; n = 155 nanobars). Colormap: blue: low; green: medium; red: high. In the upper right image, the dashed circles and square regions are used to calculate the 'end' and 'center' signals, respectively, for all nanobar images. (E) Mean intensity profile along the dashed line in (D) for all three nanobar widths. Fluorescence traces are normalized to the intensity at the center of the nanobar. Green: hPiezo1; Magenta: CellMask Deep Red. Error bars are SEM. (F) Scattered plot of the 'end' to 'center' ratio for all nanobars in both the hPiezo1 channel and the CellMask channel (Mem.). Estimated radius of curvature for the curved ends are labelled on the x-axis. *p* values given by one-way ANOVA with *post hoc* Tukey's test. ***p < 10^{-7}, **p < 10^{-3}. All scale bars are 2 µm.
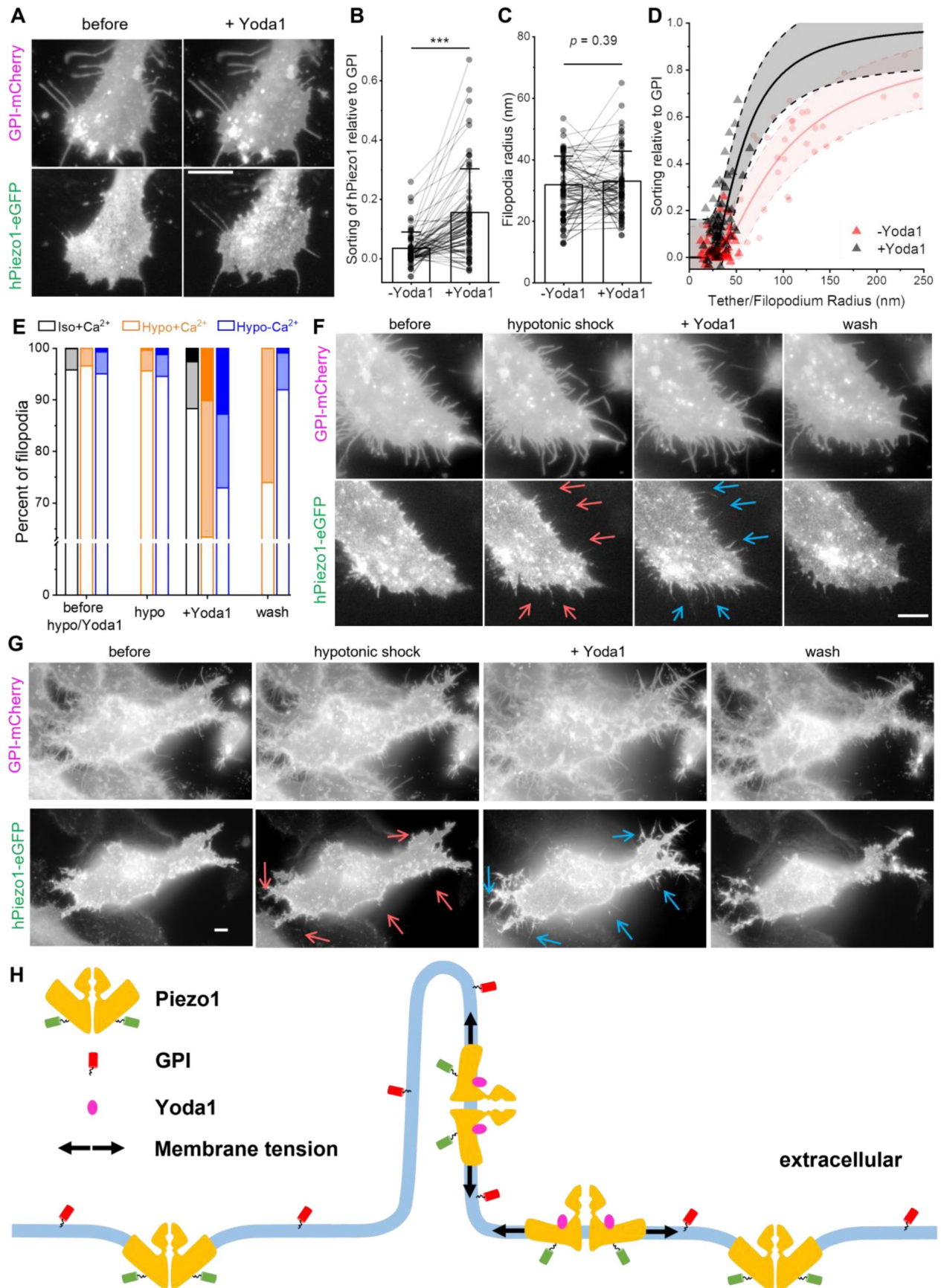
Figure 4.

Yoda1 leads to increased sorting of Piezo1 on filopodia, independent of Ca^{2+}.

(**A**) Left: fluorescence images of a HeLa cell (see Fig. S11A for the full cell) co-expressing GPI-mCherry (up) and hPiezo1-eGFP (down). Right: 10 min after adding 10 µM Yoda1 to the cell on the left. (**B, C**) Quantifications of hPiezo1 sorting on filopodia (**B**) and filopodia radii (**C**), n = 66 filopodia. p values given by paired Student's t test, ***p <10^{-7}. (**D**) S_{filo} plotted as a function of filopodia radius before (red triangle) and after (black triangle) adding Yoda1. The black line is a one-parameter fit of the +Yoda1 data to equation (1) with $\widetilde{A}_P$ fixed at 2400 nm^2. Shaded areas represent the 90% confidence interval. Fitted C_0^{-1} = (4 ± 13) . Data from Fig. 2G are shown in light red for comparison. All data points in (**B**) – (**D**) are quantified from cells cultured in regular XC and are limited to filopodia that did not significantly change positions after addition of Yoda1. (**E**) Percentage of filopodia that showed strong (S_{filo} > 0.3, dark), weak (0.1 < S_{filo} < 0.3, light), and no (S_{filo} < 0.1, open) sorting of hPiezo1 under the labelled conditions. Black: no osmotic shock, regular XC (n = 752 filopodia); Orange: hypotonic shock, regular XC (n = 564 filopodia); blue: hypotonic shock, Ca^{2+}-free XC (n = 771 filopodia). (**F, G**) Fluorescence images of HeLa cells in regular (**F**, see Fig. S11B for the full cell) and Ca^{2+}-free (**G**) XC buffer. Up: GPI-mCherry. Down: hPiezo1-eGFP. Left to right: before treatments; 10 min after swelling with regular (**F**) or Ca^{2+} free (**G**) hypotonic buffer; 20 min after adding 10 µM Yoda1 (dissolved in regular (**F**) or Ca^{2+} free (**G**) hypotonic buffer); after washing 3 times with regular (**F**) or Ca^{2+} free (**G**) XC buffer. Red/blue arrows point to the filopodia where Piezo1 signals were absent/enhanced before/after adding Yoda1. All fluorescence images here are shown in log-scale to highlight the filopodia. All scale bars are 5 µm. (**H**) Illustration showing the membrane curvature sorting of Piezo1 (orange-green) relative to GPI (red) and the effect of Yoda1(magenta circle) and pre-stressing (black arrows) on the curvature sorting of Piezo1.

Under regular cell culture conditions, we noticed that only a small portion of filopodia (~10%) showed measurably changed Piezo1 signal in response to the Yoda1 treatment (Fig. 4E). We reasoned that the opening of Piezo1 resembles a sharp two-state transition[14], and the main effect of Yoda1 is to lower the transition tension[37]. Piezo1 cannot be opened by Yoda1 if the resting tension of the cell is too low, whereas channels that are in a pre-stressed (yet closed) state would have a higher chance to respond to Yoda1. To test this, we pre-stressed the cells with hypotonic shock. The hypotonic shock itself did not significantly change the fraction of filopodia that showed significant sorting of Piezo1. However, significantly more (~35%) filopodia responded to a subsequent Yoda1 treatment (Fig. 4E, 4F, S11B, S12C). Importantly, Yoda1-induced S_{filo} of Piezo1 is not a result of Ca^{2+} influx, as a similar effect can be observed on cells maintained in a Ca^{2+}-free buffer (Fig. 4E, 4G). Additionally, Yoda1 induced sorting of Piezo1 is reversible as Piezo1 signals disappear from filopodia after washing out Yoda1 (Fig. 4E-G). Importantly, shear stress applied during washing steps alone did not significantly change the sorting of Piezo1 on filopodia (Fig. S12D). On individual filopodium, the apparent all-or-none response to Yoda1 treatment suggests that cooperativity between Yoda1-Piezo1 or Piezo1-Piezo1 may also play a role in modulating the channel's curvature sorting behavior. The flattening of Piezo1 during activation has been suggested using HS-AFM[11], in silico[48,49], and has recently partially been confirmed using CryoEM[10]. Our study suggests this conformational change of Piezo1 may also happen in live cells (Fig. 4H).

Piezo1 inhibits filopodia formation

Curvature sensing proteins often have a modulating effect on membrane geometry. For example, N-BAR proteins, which strongly enrich to positive membrane curvature, can mechanically promote endocytosis by making it easier to form membrane invaginations[40,50]. Thus, we hypothesize that Piezo1, which strongly depletes from negative membrane curvature (Fig. 1, Fig. 2), can have an inhibitory effect on the formation of membrane protrusions such as filopodia.

Indeed, HeLa cells with higher expression level of hPiezo1-eGFP tend to have less filopodia (Fig. 5A ⤢, 5B ⤢). However, due to the low expression of hPiezo1-eGFP in the majority of HeLa cells, only a weak negative correlation was observed between filopodia number and hPiezo1-eGFP fluorescence in each cell (Fig. 5B ⤢). In HEK293T cells where hPiezo1-eGFP expresses 3.5-fold higher, a stronger negative correlation was observed between the number of filopodia per cell and hPiezo1-eGFP density on the cell membrane (Fig. 5C ⤢, 5D ⤢). Interestingly, the negative correlation almost completely diminished when HEK293T cells were cultured in 5 μM Yoda1 (Fig. 5D ⤢), consistent with Yoda1's ability to reduce the curvature effects of Piezo1 (Fig. 4 ⤢). In Piezo1 knockout (Piezo1-KO) cells, adding Yoda1 to the culture medium does not significantly change the number of filopodia (Fig. 5E ⤢), suggesting the agonist does not directly regulate filopodia formation without acting on Piezo1.
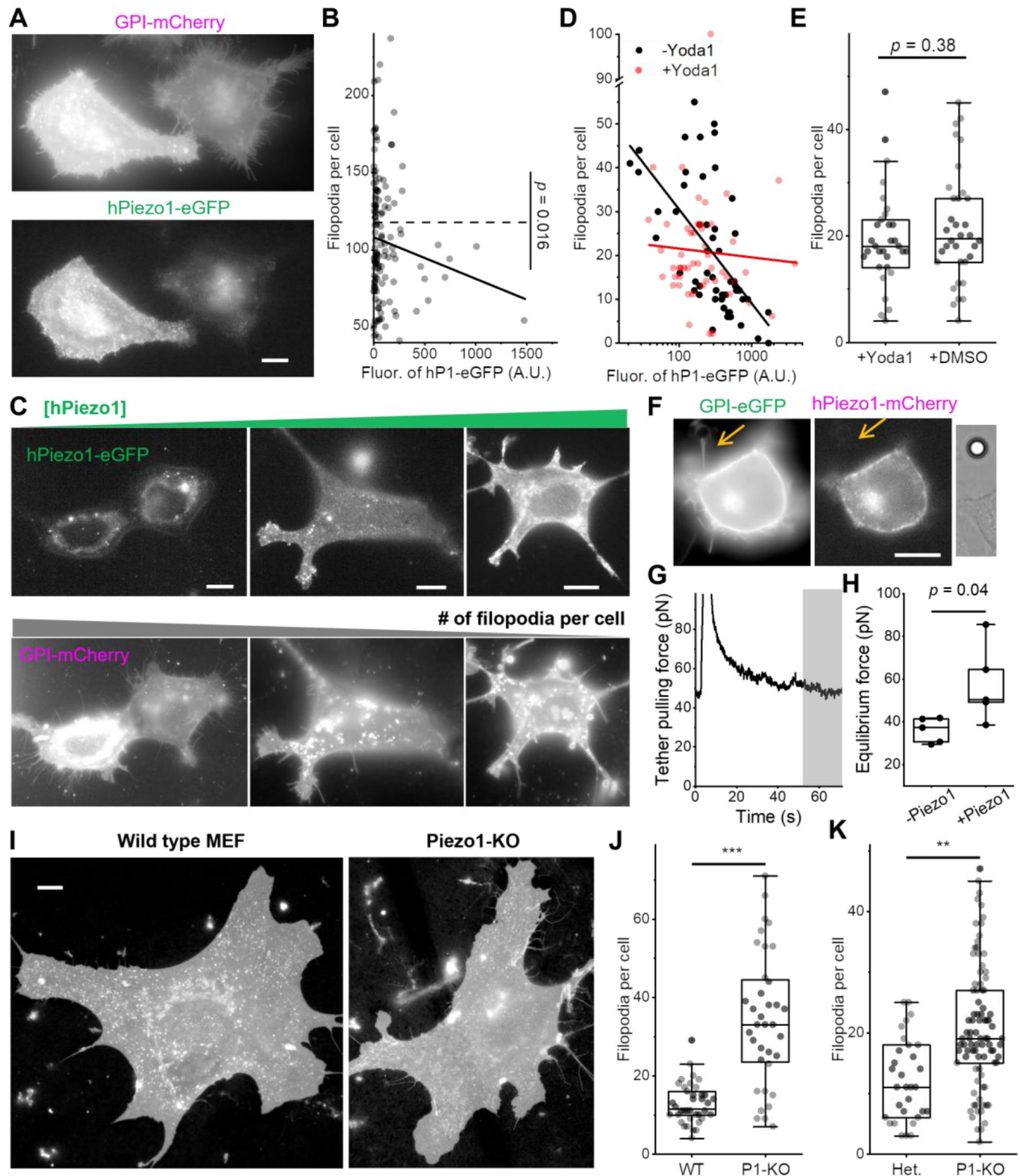
Figure 5.

Piezo1 inhibits filopodia formation.

(A) Fluorescence images of HeLa cells co-expressing GPI-mCherry (up) and hPiezo1-eGFP (down). **(B)** Relation between the number of filopodia and hPiezo1-eGFP expression level in HeLa cells (n = 129 cells). Dash line represents the average number of filopodia per cell. Solid line represents a linear fit (Pearson's r = −0.13). **(C)** Fluorescence images of HEK293T cells coexpressing hPiezo1-eGFP (up) and GPI-mCherry (down). Cells are arranged so that the expression level of hPiezo1-eGFP increases from left to right, the number of filopodia per cell decreases correspondingly. **(D)** Relation between the number of filopodia and hPiezo1-eGFP expression level in HEK293T cells cultured in regular (black, n = 52 cells) and 5 µM Yoda1 containing (red, n = 50 cells) media. Lines are linear fits between y and log(x). Without Yoda1 (black): slope = −21.5 ± 4.0, Pearson's r = −0.61. With Yoda1 (red): slope = −2.0 ± 5.0, Pearson's r = −0.06. **(E)** The number of filopodia per Piezo1-KO MEF incubated with 5 µM Yoda1 (n = 31 cells) or 0.1% DMSO (n = 34 cells). **(F)** A HEK293T cell co-expressing hPiezo1-eGFP (left) and GPI-mCherry (middle), with a tether (arrow) pulled by an optically-trapped bead (right). **(G)** Time dependent pulling force for the tether in (**F**). The tether was stretched at t = 3 s. The gray area was used to calculate the equilibrated pulling force. **(H)** Equilibrium tether pulling force for HEK293T cells only expressing GPI-eGFP (-Piezo1) or co-expressing hPiezo1-mCherry and GPI-eGFP (+Piezo1). **(I)** Representative (of the median number of filopodia per cell) fluorescence images of WT (left) and Piezo1-KO (right) MEF, both stained with CellMask Deep Red. MEFs were from littermate embryos that were dissected on the same day. **(J)** The number of filopodia per cell for WT (n = 38 cells) and Piezo1-KO (P1-KO; n = 36 cells) MEFs from a pair of littermates. Cells were imaged 30 days after dissection (3 passages). **(K)** The number of filopodia per cell for Het. (n = 32 cells) and P1-KO (n = 89 cells) MEFs from a pair of littermates. Cells were imaged 52 days after dissection (6 passages). All fluorescence images here are shown in log-scale to highlight the filopodia. All scale bars are 10 µm. *p* values given by two-tailed Student's *t*test after checking for normality. ***p < 10^{-7} **p < 10^{-3}.

Next, we quantified the mechanical effect of Piezo1 by measuring the force needed to maintain 5 ~ 10 µm tethers from HEK293T cells (Fig. 5F, 5G). The equilibrium tether pulling force from cells overexpressing hPiezo1 was 58 ± 18 pN (mean ± SD, n = 5), significantly higher than cells without hPiezo1 overexpression (36 ± 6 pN; mean ± SD, n = 5; Fig. 5H). Overexpressed Piezo1 in HEK293T cells (Fig. 5D – 5H) is ~3.5-fold higher than in HeLa cells (Fig. 5A – 5B), thus ~10-fold of the endogenous level (Fig. S5C). While this high Piezo1 level may resemble the local density of Piezo1 at specific cellular regions such as focal adhesion sites[27], we wonder whether the observed mechanical effect on membrane protrusions can be of general physiological relevance. To answer this question, we compared the number of filopodia on MEFs dissected from wild type (WT) or Piezo1 heterozygous (Het.) mice with those from their Piezo1-KO littermates (Fig. 5I)[25,28]. Both WT (Fig. 5J) and Het. (Fig. 5K) MEFs showed significantly less filopodia compared to their Piezo1-KO counterparts, suggesting that endogenous level Piezo1 can already inhibit filopodia formation.

Discussion

The curved structure of Piezo1 trimer has been suggested to play an important role in the activation of the channel[7,10,11,14]. Our study demonstrates that the coupling of Piezo1 to nanoscale membrane curvature also regulates the distribution of Piezo1 within the plasma membrane. The observations of Piezo1 depletion from membrane protrusion (Fig. 1, Fig. 2) and enrichment to membrane invaginations (Fig. 3) are consistent with a recent report of Piezo1 distribution in red blood cells[19]. Our experiments also strongly support the hypothesis that Piezo1 flattens during activation[7,10,11,37], thereby coupling the activation of the channel to its subcellular distribution. It is worth noting that our data and model do not assume

any molecular detail of Piezo1 and are limited by optical resolution (~500 nm). However, the revealed nano-geometries of the channel are on the order of 10 nm and are in surprising agreement with the structural information of purified Piezo1 trimers[7], [8], [10], [11].

Membrane curvature sensing has been studied for a range of proteins including BAR domain proteins and GPCRs[34],[40],[45],[51], our report extends such quantitative studies to a mechanosensitive ion channel. Our parsimonious model predicts that the large area of the Piezo1-membrane complex (more than 10-fold larger than a typical GPCR) leads to prominent size effects that has often been neglected when studying smaller membrane proteins (Fig. S10): 1) sorting of Piezo1 is exquisitely sensitive to the flattening of the channel (C_0 from 83^{-1} nm^{-1} to 0 nm^{-1}). On 50 nm protrusions, the model predicts a ~200% increase in sorting when Piezo1 flattens. This effect diminishes to ~10% if Piezo1 were 10 times smaller; 2) Piezo1 would deplete from highly curved invaginations ($S < 1$ when $R_i < 41$ nm) due to the large energy cost to match the spontaneous curvature of Piezo1 with the shape of the invaginations. The second prediction may be verified by systematically studying Piezo1 density on highly curved membrane invaginations. However, it is worth noting that we assumed a zero spontaneous curvature for membranes associated with Piezo1 and that the spontaneous curvature of the Piezo1-membrane complex is independent of the shape of surrounding membranes. These assumptions may no longer hold when studying Piezo1 in highly curved invaginations or liposomes[11]. Furthermore, our model assumes that Piezo1 behaves as 2-dimensional ideal gas in the membrane. While the assumption is consistent with the observation that Piezo1 trimers function independently[52], we did neglect potentially important intermolecular interactions between Piezo1 trimers[25],[28],[49],[53]. Notably, apparent clusters of Piezo1 were often observed on cell membranes (Fig. 1, Fig. S1-S5) and on membrane tethers (Fig. 2D), suggesting that attractions between Piezo1 trimers may also be important for controlling the detailed distribution of the channel in cells. Lastly, Piezo1-membrane complexes likely have isotropic curvatures (such as a spherical dome[7]), whereas the membrane protrusions and invaginations in our study are anisotropically curved, with one principal membrane curvature close to zero. Improved models that consider the effect of curvature anisotropy may provide additional insights to the curvature sensing of Piezo1[54],[55].

In addition to membrane curvature, tension in the membrane may also affect the subcellular distribution of Piezo1[21]. Particularly, membrane tension can activate the channel and potentially change Piezo1's nano-geometries. This tension effect is unlikely to play a significant role in our interpretation of the curvature sorting of Piezo1 (Fig. 2): (1) HeLa cell membrane tension as probed by short tethers (Fig. S9F; 45 ± 29 pN/ µm on blebs and 270 ± 29 pN/ µm on cells, with the highest recorded tension at 426 pN/ µm) are significantly lower than the activation tension for Piezo1 (> 1000 pN/µm[12],[13],[23],[56]). (2) With more activated (and potentially flat) channels under high membrane tension, one would expect a higher density of Piezo1 on tethers pulled from tenser blebs. This is the opposite to our observations in Fig. 2C – 2G, where Piezo1 density on tethers was found to decrease with the absolute curvature, thus tension (eq. S6), of membrane tethers.

A Yoda1-induced flattening of Piezo1 has not been directly observed via CryoEM. Our results (Fig. 4) point towards two challenges in determining this potential structural change: (1) Yoda1 induced changes in Piezo1 sorting is greatly amplified after pre-stretching the membrane (Fig. 4E), pointing to the possibility that a significant tension in the membrane is required for the flattening of Yoda1-bound Piezo1. (2) Piezo1 is often incorporated in small (< 20 nm radius) liposomes for CryoEM studies. The shape of liposomes can confine the nano-geometry of Piezo1[10],[11], rendering it significantly more challenging to respond to potential Yoda1 effects. This potential influence of membrane curvature on the activation of Piezo1 would be an interesting direction for future studies.

The antagonistic effect of Piezo1 on the formation of filopodia is consistent with several recent observations: First, Piezo can modulate the morphogenesis and targeting of dendrites independently of its activity as a mechanosensitive ion channel[57]. Secondly, knocking out Piezo in Drosophila promotes axon regeneration[58]. Furthermore, Piezo1 negatively regulates the morphological activity (i.e., number of protrusions) of muscle stem cells[59]. Lastly, Piezo2 inhibits neurite outgrowth in N2A cells[17]. In addition to membrane curvature, several parallel Piezo-related mechanisms can regulate the formation and growth of filopodia, including Ca^{2+} signaling induced by the activation of Piezo and potential interactions between specific Piezo domains with cytoskeletal components[17],[58],[59]. Our data do not exclude these parallel mechanisms, rather, we suggest that the curvature preference of Piezo1 provides an additional route to control filopodia dynamics. Further studies are required to fully dissect the contribution of each of these variables.

In addition to regulating the formation of filopodia (Fig. 4), the curvature sensing of Piezo1 can have a direct benefit of making sure that the protein is retained at the rear edge during cell migration and to avoid losing Piezo1 to retraction fibers (e.g., Fig. S4B)[28]. Moreover, the dynamics of filopodia are often linked to the metastatic transition of cancer cells[41], suggesting new roles of Piezo1 in cancer biology[29].

Overall, our study suggests that the curvature sensing of Piezo1 provides nanoscale input for the channel in live cells and is a universal regulator of the channel's distribution within cell membranes. These features are likely to be of fundamental importance to a wide range of Piezo1-dependent biological processes.

Methods

Cell harvesting and culture, transfection, bleb formation, osmotic shock, and Yoda1 treatment

HeLa cells (ATCC and from Renping Zhou lab, Rutgers) were cultured in Eagle's Minimum Essential Medium (EMEM) supplemented with 10% Fetal Bovine Serum (FBS) and 1% Penicillin/Streptomycin (PS). HEK293T cells (from Zhiping Pang lab, Rutgers) were cultured in Dulbecco's Modified Eagle Medium (DMEM) supplemented with 10% FBS, 1% PS and 1% Sodium Pyruvate. Both cell lines were seeded in 100 mm plastic dishes with ~ 1×10^6 cells per dish. Cells were kept in incubator with 5% CO2 and 100% relative humidity at 37°C.

All animal studies were approved by the Institutional Animal Care and Use Committee of University of California at Irvine and performed in accordance with their guidelines. To obtain Mouse Embryonic Fibroblasts (MEFs), mice that are heterozygous for Piezo1 knockout (Piezo1$^{\Delta/+}$) were obtained from Jackson Laboratories (JAX stock 026948) and were bred with C57BL6/J to maintain the colony. Piezo1$^{\Delta/+}$ mice were bred with each other to generate a mixture of wild type (WT), heterozygous (Het.), and knockout (Piezo1-KO) embryos. Mice were considered embryonic day 0.5 upon vaginal plugging. Embryos were genotyped via a commercial vendor (Transnetyx). MEFs with endogenously labelled Piezo1 were harvested from Piezo1-tdTomato reporter mice (*Mus. musculus*, JAX stock 029214), expressing Piezo1 with a tdTomato knock-in at the C-terminus (gift from Patapoutian lab)[60].

Embryos were dissected by separating the head, limbs, and tail from the embryo at embryonic days 10.5 (WT, Het, Piezo1-KO) or 12.5 (Piezo1-tdTomato) in Dulbecco's PBS (Gibco) supplemented with 33 mM D-(+)-glucose (Sigma-Aldrich) and 1% Penicillin-Streptomycin (10,000 U/mL; Gibco). Following dissection, tissue was spun down at ~260G for 5 min, and the supernatant was aspirated. The remaining tissue from each embryo was gently triturated in DMEM (ThermoFisher Scientific) with 15% FBS (Omega Scientific), 1x GlutaMax (ThermoFisher Scientific), 1 mM sodium pyruvate

(ThermoFisher Scientific), and 1x non-essential amino acid solution (ThermoFisher Scientific) in a sterile environment to obtain single cells. All MEFs were grown in a 5% CO2 incubator at 37 °C, and media was changed 24 hours after plating. Cells from individual embryos obtained from the Het. crosses were cultured separately in 12-well plates (USA Scientific) coated with 0.1% gelatin solution (Fisher Scientific) until genotypes were determined. Subsequently, cells were pooled together by genotype and cultured. Cells were grown until 90% confluency was reached. All MEFs were passaged using TrypLE Express (ThermoFisher) to dissociate the cells and were spun at ~260G for 5 min. Cells were passaged at least three times prior to use in experiments.

For fluorescence imaging, cells were transfected in 35 mm plastic dishes at around 60% confluency. For HeLa cells, a mixture of 125 μL Opti-MEM, 3.5 μL TransIT-X2 and 300 ng of each plasmid DNA were added after 12 min incubation. For MEFs and HEK293T cells, a mixture of 250 μL Opti-MEM, 5 μL P3000 reagent, 3.5 μL Lipofectamine reagent and 500 ng of each plasmid DNA were added after 15 min incubation. Cells were kept in an incubator for 24 hours before further split onto 35 mm precoated (Poly-D-Lysine for HeLa cells and Matrigel for MEFs and HEK293T cells) glass bottom dishes (Cellvis) for imaging. Cells were imaged 12-48 hours after splitting.

Before imaging, cell culture medium was replaced with extracellular imaging buffer (XC buffer) containing 125 mM NaCl, 2.5 mM KCl, 15 mM HEPES, 30 mM Glucose, 1 mM MgCl2 and 3 mM CaCl2 with pH 7.3. Ca^{2+} free experiments were done by omitting CaCl2 in the XC buffer. Hypotonic osmotic shock was carried out by using a diluted XC buffer that is 0.25 ~ 0.5 of its initial concentration.

To trigger blebs, HeLa cells were incubated with 400 μL of 100 ~ 200 μM Latrunculin B (diluted in XC buffer) for 5 min. Additional XC buffer was added after bleb formation to keep a final Latrunculin concentation of 20 ~ 40 μM during experiments.

For experiments in Fig. 5, stock solution of Yoda1 (5 mM, dissolved in DMSO) was diluted to 5 μM in EMEM before use. Cells were incubated with 5 μM Yoda1 solution for 2 to 4 hours. Control group was incubated with 0.1% DMSO for the same amount of time. After incubation, culture media were carefully replaced with XC buffer containing the same concentrations of Yoda1 or DMSO. For experiments in Fig. 4, stock solution of Yoda1 was diluted to 10 μM in XC buffer before use. The number of filopodia per cell in Fig. 5 was counted manually for all protrusions that are longer than 1 μm for HEK293T cells and longer than 2 μm for MEFs and HeLa cells, counting was independently verified by two researchers and by FiloDetect[61].

Imaging, tether pulling, and quantification

Fluorescence imaging was done on either a Leica DMi8 or a Nikon Ti2-A inverted microscope. Leica DMi8 was equipped with an oil-immersion objective (100X; NA 1.47; Leica) and laser excitation (488 nm for eGFP and 561 nm for mCherry, tdTomato, or mOrange2), and allows total internal reflection fluorescence (TIRF) imaging. Nikon Ti2-A microscope was equipped with LED excitation (~470 nm for eGFP and ~550 nm for mCherry, tdTomato, or mOrange2) and with either a water-immersion objective (60X; NA 1.20; Nikon) or an oil-immersion objective (100X; NA 1.30; Nikon). The oil immersion objective was integrated with an objective heater (OKO lab) for 37°C measurements. Temperature was calibrated by directly measuring the temperature of the medium near the imaged cell. The Leica DMi8 was integrated with an Infinity Scanner (Leica) for fluorescent recovery after photobleaching (FRAP) experiments. The Nikon Ti2-A microscope was integrated with two micromanipulators (PatchPro-5000, Scientifica) and an optical tweezer (Tweez305, Aresis) for tether pulling and force measurements. Images were analyzed with ImageJ and Matlab (R2019a).

Membrane tethers were pulled from the cell body or cell-attached membrane blebs using either a motorized micropipette[62] with a fused tip or a polystyrene bead (4.5 μm) trapped with an optical tweezer.

Membrane curvature sorting and filopodia/tether radii were calculated according to the illustration in Fig. S3. We hypothesize that filopodia and membrane tether are cylindrical membrane tubes, and that the quantum yields of fluorescent proteins are independent of local curvature. For radius calculation, we also assume that both bilayers of a flat region of the cell are captured in widefield epi-fluorescence images[23].

For membrane tube with a diffraction-limited radius r, if a region of interest (ROI) is drawn to cover a length L of the tube (Fig. S3B), the total membrane area with the ROI is given by

$$A_{\text{tube}} = 2\pi r L \quad (\text{eq. S1})$$

Assume I_{mean}^{tube} is the background-corrected mean fluorescence within the ROI on the tube, A_{ROI} is the area of the ROI, the total fluorescence should equal to the number density of FPs on membrane (ρ) multiplied by A_{tube} and by the fluorescence per FP (β).

$$I_{\text{mean}}^{\text{tube}} \cdot A_{\text{ROI}} = A_{\text{tube}} \cdot \rho \cdot \beta \quad (\text{eq. S2})$$

The background-corrected mean fluorescence within the ROI on a flat region of the cell membrane (Fig. S3B), I_{mean}^{cell}, is related to ρ and β by

$$I_{\text{mean}}^{\text{cell}} = M \cdot \rho \cdot \beta \quad (\text{eq. S3})$$

The factor M takes into account the number of cell membrane surfaces within the imaging depth.

Combining equations S1 to S3, the radius of the membrane tube is given by

$$r = \frac{M \cdot I_{\text{mean}}^{\text{tube}} \cdot A_{\text{ROI}}}{2\pi L \cdot I_{\text{mean}}^{\text{cell}}} \quad (\text{eq. S4})$$

When imaging a flat region of the cell under widefield fluorescence microscopy, we use $M = 2$ (Fig. S3D). HEK293T cells often do not contain a flat region on the cell body (Fig. S2E, Fig. S4). To address this issue, we use TIRF microscopy and set $M = 1$ when measuring filopodia radii from HEK293T cells.

In principle, r can be calculated using the fluorescence of any membrane proteins/lipids, however, only molecules in the membrane that do not have membrane curvature sensitivity can give the real tube radius. The reported tether and filopodia radii in our study were determined using the fluorescence of GPI-FP. GPI anchors the FP to the outer leaflet of the plasma membrane. Due to the relatively large size of FP to the GPI anchor, GPI-FPs may have enrichment towards highly curved protrusions[63]. For the same reason, CaaX-FP, which is anchored to the inner leaflet of the plasma membrane may deplete from membrane protrusions. However, we expect this effect to be less than 7%, as the relative sorting of CaaX to GPI was measured to be 0.863 ± 0.008 (Fig. 1D).

When a tether is pulled from a bleb (Fig. 3C and 3D), an apparent radius of the tether was calculated using the background-corrected mean fluorescence within the ROI of the bleb membrane instead of I_{mean}^{cell} (Fig. S3C).

Membrane curvature sorting (S) on a protrusion is the effective number density of a molecule of interest (MOI) on the membrane tube relative to either a flat region on the cell body (Fig. S3B) or the membrane bleb (Fig. S3C).

$$S = \frac{r(\text{MOI})}{r(\text{GPI})} \quad (\text{eq. S5})$$

$S = 0$ when the MOI is completely depleted from the tube. $S = 1$ when the MOI has the same curvature preference as the GPI-FP reference.

An ROI width of 0.5 µm was used for all tether/filopodium quantifications. Filopodia that are sufficiently away (> 1 µm) from other membrane structures and more than 3 µm in length were picked for calculating S and r. Errors in S and r were propagated using the standard deviation in the background fluorescence as the error for mean fluorescent intensities. In Fig. 4E, filopodia with clear Piezo1 signal on less than 10% of the total length (typically corresponding to $S < 0.1$) were considered as no response; between 10% to 50% of the filopodia (typically corresponding to $0.1 < S < 0.3$) were considered weak response; more than 50% of the filopodia ($S > 0.3$) were considered strong response.

Fabrication, cell culture, imaging, analysis with nanobar-substrates

Nanobar substrates were fabricated on the surface of a square quartz coverslip with electron-beam lithography (EBL)[35],[36]. Briefly, the quartz chip was firstly spin-coated with the poly(methyl methacrylate) (PMMA) (MicroChem) with around 300 nm height, followed by one layer of conductive polymer AR-PC 5090.02 (Allresist). Nanobar patterns were written by Electron Beam Lithography (FEI Helios NanoLab), and then developed in isopropanol: methylisobutylketone solution with 3:1 ratio. After that, a 30 nm thickness chromium (Cr) mask was deposited by thermal evaporation (UNIVEX 250 Benchtop) and then lifted off with acetone. Nanobars were then generated through reactive ion etching (RIE) with a mixture of CHF3 and CF4 (Oxford Plasmalab). Nanobar dimensions were identified by scanning Electron Microscopy (FEI Helios NanoLab) imaging with 10 nm Cr coating.

To enable cell imaging on nanochip, the chip was attached to the 35 mm cell culture dish (TPP) with a hole punched in the center to expose nanobar pattern. Before cell plating, the dish substrate was sterilized by UV treatment for 20 minutes and treated with high-power air plasma (Harrick Plasma) for 3 minutes. The surface was coated with 0.2% Gelatin (Sigma-Aldrich) for 30 minutes to promote cell attachment. Homosapiens bone osteosarcoma U2OS cells (ATCC) maintained in DMEM with GlutaMAX (Gibco) supplemented medium with 10% FBS (Life Technologies) and 1% Penicillin-Streptomycin (PS) (Life Technologies) were then cultured on the nanobar chip one day before transfection. The cells were maintained in a standard incubator under 37°C and 5% CO_2. Cells were transfected with hPiezo1-eGFP plasmid via Lipofectamine. Membrane staining with CellMask Deep Red (Life Technologies) was performed before imaging. The 1000-time diluted dye was added to the cells and incubated for 1 minutes at 37°C and washed with DMEM.

Cell imaging was performed with a spinning disc confocal (SDC) built around a Nikon Ti2 inverted microscope containing a Yokogawa CSU-W1 confocal spinning head and a 100 X/1.4NA oil immersion objective. eGFP was excited at 488 nm and detected at 505-545 nm. CellMask Deep Red was excited at 639 nm and detected at 672-712 nm. During imaging, the cells were maintained under 37°C with 5% CO_2 in an on-stage incubator.

The Piezo1-eGFP curvature sensing preference on gradient nanobars with different widths was quantified using Matlab[35],[36]. In brief, the background signals of each image were firstly subtracted by the rolling ball algorithm in ImageJ (radius = 0.77 µm). Next, the nanobars covered by cell membrane were identified by square masks (3.92 µm × 3.92 µm) centered at the nanobar. The average images were generated by averaging all the individual nanobar masks. To quantify the end-to center ratio, each nanobar was segmented into three ROIs (two nanobar-ends and a nanobar-center; Fig. 3D). End-to-center ratios were calculated by dividing the mean end-intensity with the mean center-intensity. The curvature sorting of Piezo1 on membrane invaginations is evaluated by dividing the end-to-center ratio in the Piezo1 channel by that of the CellMask channel.

Tether force measurement

To measure tether force, a membrane tether is pulled by a bead trapped with an optical tweezer (Tweez305, Aresis) equipped on the Ti2-A inverted microscope (Nikon). Membrane tubes were pulled to around 10 μm in length and then held until an apparent equilibrium force f was reached (Fig. S9). Then fluorescence images of the cell and the tether were taken for tether radius (r) measurements according to eq. S4 ⧉. Force on the bead was calculated from the displacement of the bead from the center of the trap and the trap stiffness (calibrated before each experiment by applying equipartition theorem to the thermal fluctuation of a trapped bead). Then membrane tension σ and bending stiffness κ_m were be calculated by:[43]⧉

$$\sigma = \frac{f}{2\pi r} \quad (\text{eq. S6})$$

$$\kappa_\text{m} = \frac{fr}{2\pi} \quad (\text{eq. S7})$$

Note that the pulling force f may contain contributions from the cytoskeleton and membrane asymmetry. Therefore, a more accurate measure of κ_m is to fit $f/2\pi$ vs. r^{-1} to a linear relation where the slope will report κ_m and the intercept will report the aforementioned additional contributions to tether pulling force (Fig. S9F).

FRAP measurements

3 to 6 circular ROIs with radius R_bleach = 1.5 μm were picked on flat regions of HeLa cell expressing hPiezo1-eGFP. 488 nm laser at full power was used to photo bleach the selected ROI for ~ 1 s. Frames before photobleaching and the first frame after photobleaching were used to normalize the fluorescence intensity, background photobleaching was corrected by tracking the fluorescence of the entire cell. The normalized recovery curve $I(t)$ was fitted to the following relation to extract half-recovery time ($\tau_{0.5}$, 2-parameter fit):

$$I(t) = \frac{I_0 + \frac{t}{\tau_{0.5}}}{1 + \frac{t}{\tau_{0.5}}} \quad (\text{eq. S8})$$

The diffusion coefficient was calculated by[23]⧉,[64]⧉:

$$D_\text{cell} = 0.224 \frac{R_\text{bleach}^2}{\tau_{0.5}} \quad (\text{eq. S9})$$

Model for the curvature sorting of Piezo1

We assume the protein-membrane complex has a preferred curvature C_0. In the case of Piezo1, each protein unit would correspond to a trimer of Piezo1 with associated membranes, C_0 represents a balanced shape between the curvature preference of the Piezo1 trimer and the preferred shape of the associated membrane. If we define protrusions (e.g., tethers, filopodia) on the cell to have a negative curvature, then C_0 would be predicted to be positive for Piezo1-membrane complex, assuming that the associated membranes prefer to be flat.

The energy of putting one unit of protein-membrane complex into a membrane of curvature K:

$$E^\text{b} = \frac{1}{2}\tilde{\kappa}A_\text{P}(K - C_0)^2 \quad (\text{eq. S10})$$

K is the sum of principle curvatures of the membrane surface. For a flat membrane, $K = 0$; for tubular membrane protrusions of radius R_p (e.g., filopodia, tether), $K = -1/R_\text{p}$; for tubular membrane invaginations of radius R_i, $K = 1/R_\text{i}$. Here, we ignored the contribution of Gaussian curvature (the product of principle curvatures) which is expected to be a constant that only

depends on the boundary conditions (Gauss-Bonnet theorem)[65]. A_p is the area of the proteinmembrane complex. $\tilde{\kappa}$ is the bending stiffness of the protein-membrane complex, which represents the stiffness when bending the membrane (κ_m) and the protein (κ_p) in series:

$$\frac{1}{\tilde{\kappa}} = \frac{1 - \theta_p}{\kappa_m} + \frac{\theta_p}{\kappa_p} = \frac{1}{\kappa_m} + \theta_p \left(\frac{1}{\kappa_p} - \frac{1}{\kappa_m} \right) \quad \text{(eq. S11)}$$

Here, ι_p is the area fraction of the protein in each unit of protein-membrane complex. Measurements of the overall membrane bending stiffness of Piezo1 expressing cells (~κ_m), therefore serve as a good estimation for $\tilde{\kappa}$ when either θ_p is small or when $\kappa_p \approx \kappa_m$. A recent study suggests that Piezo1 is surprisingly flexible, presenting a bending stiffness similar to that of the lipid membrane[66].

The energy difference between a protein on the curved membrane versus the same protein on a flat membrane:

$$\Delta E = E^b(\text{curved}) - E^b(\text{flat}) = \frac{1}{2} \tilde{\kappa} A_P (K - C_0)^2 - \frac{1}{2} \tilde{\kappa} A_P (C_0)^2 = \frac{1}{2} \tilde{\kappa} A_P (K^2 - 2C_0 K) \quad \text{(eq. S12)}$$

ΔE describes the energy change of moving a protein-membrane complex from a flat membrane to a curved membrane, where the flat-curve membrane geometry was pre-equilibrated (e.g., a tube pulled from a piece of flat membrane and is held by an external force). Note that the model predicts an energy cost of moving a 'flat protein' (C_0 =0) from a flat to a curved region, this is because the 'flat protein' will deform the pre-equilibrated curvature, with an energy cost that is larger for bigger proteins. The reference molecule GPI has a much smaller area in the membrane (~1 nm^2[ ]) compared to Piezo1, therefore ΔE for GPI is negligible.

Assume the proteins in the membrane can be approximated as 2D ideal gas (i.e., no interaction between proteins, density of protein on the membrane is low). The density of the protein on the curved membrane relative to its density on the flat membrane follows the Boltzmann distribution:

$$S = \exp(\frac{-\Delta E}{k_B T}) = \exp\left[-\frac{\tilde{\kappa} A_P}{2 k_B T} (K^2 - 2C_0 K) \right] \quad \text{(eq. S13)}$$

Note that eq. S13 is essentially the same as equation 8 of ref.[34] or equation 2 of ref.[45] (under low protein density and negligible protein-protein interaction), where free energy-based derivations were presented. For membrane protrusions of radius R_p, $K = -1/R_p$:

$$S = \exp\left[-\frac{\tilde{\kappa} A_P}{2 k_B T} \left(\frac{1}{R_p^2} + \frac{2C_0}{R_p} \right) \right] \quad \text{(eq. S14)}$$

which was used to fit the sorting of Piezo1 on membrane tethers (Fig. 2G; eq. 1) using OriginPro (2020). The resulted fitting parameters were, $\tilde{\kappa} A_P$ = 4800 k_BT·nm^2 and C_0^{-1} = 83 nm, corresponding to the nano-geometry of Piezo1-membrane complex under a resting state. Fix $\tilde{\kappa} A_P$ = 4800 k_BT·nm^2 and fit the data in Fig. 3D (+Yoda1) to eq. S14, we get C_0 = 0 nm^{-1}, potentially corresponding to the nano-geometry of Piezo1-membrane complex under open or inactive state.

For membrane invaginations of radius R_i, $K = 1/R_i$:

$$S = \exp\left[-\frac{\tilde{\kappa} A_P}{2 k_B T} \left(\frac{1}{R_i^2} - \frac{2C_0}{R_i} \right) \right] \quad \text{(eq. S15)}$$

Note that in eq. S14, S is a monotonic increasing function of protrusion radius R_p. However, the sorting of Piezo1 on membrane invaginations (eq. S15) peaks at invagination radius R_i = 1/C_0 (Fig. S10). Fig. S10 also shows that the effect of channel opening on Piezo1 sorting (changing C_0 from 83^1 nm^{-1} to 0 nm^{-1}) would almost diminish if Piezo1 were 10 times smaller. Lastly,

curvature sensing of the 10-time smaller protein on membrane invaginations would be significantly stronger if the protein also has a 10-time larger spontaneous curvature C_0 (8.3^{-1} nm^{-1}), similar to those of typical BAR domain proteins[40],[45].

Supporting information

Supplementary Figures S1-S12

Data availability

The data that support the findings of this study are available from the corresponding author upon reasonable request.

Acknowledgements

Author contributions

Z.S. and C.D.C. conceived the project. S.Y. carried out the majority of the experiments and analyzed the data. X.M., X.G., and W.Z. designed and carried out the measurements in Fig. 3.

S.A. carried out parts of the measurements in Fig. 4 and Fig. S12. B.L. carried out parts of the measurements in Fig. 5, Fig. S4, and Fig. S9. A.T.L. and M.M.P. designed and prepared Piezo1-KO, Piezo1-heterozygous, Piezo1-tdTomato, and wild type MEFs. H.W. helped with confocal imaging and the preparations of HEK293T cells and plasmids. M.W. helped with the imaging of D2R expressing cells and the theoretical modeling. Z.S. oversaw the experiments and data analysis of the entire project. Z.S., S.Y., and C.D.C. wrote the manuscript with input from all authors.

Declaration of Interests

The authors declare no competing interests.

References

1.   Coste B., et al. (2010) **Piezo1 and Piezo2 are essential components of distinct mechanically activated cation channels** *Science* **330**:55–60 Google Scholar

2.   Coste B., et al. (2012) **Piezo proteins are pore-forming subunits of mechanically activated channels** *Nature* **483**:176–181 Google Scholar

3.   Kefauver J. M., Ward A. B., Patapoutian A. (2020) **Discoveries in structure and physiology of mechanically activated ion channels** *Nature* **587**:567–576 Google Scholar

4.   Murthy S. E., Dubin A. E., Patapoutian A. (2017) **Piezos thrive under pressure: mechanically activated ion channels in health and disease** *Nature Reviews Molecular Cell Biology* **18**:771–783 Google Scholar

5.   Handler A., Ginty D. D. (2021) **The mechanosensory neurons of touch and their mechanisms of activation** *Nature Reviews Neuroscience* **22**:521–537 Google Scholar

6.   Ge J., et al. (2015) **Architecture of the mammalian mechanosensitive Piezo1 channel** *Nature* **527**:64–69 Google Scholar

7.   Guo Y. R., MacKinnon R. (2017) **Structure-based membrane dome mechanism for Piezo mechanosensitivity** *Elife* **6**:e33660 Google Scholar

8.   Saotome K., et al. (2018) **Structure of the mechanically activated ion channel Piezo1** *Nature* **554**:481–486 Google Scholar

9.   Zhao Q., et al. (2018) **Structure and mechanogating mechanism of the Piezo1 channel** *Nature* **554**:487–492 Google Scholar

10. Yang X., et al. (2022) **Structure deformation and curvature sensing of PIEZO1 in lipid membranes** *Nature* :1–7 Google Scholar

11. Lin Y., et al. (2019) **Force-induced conformational changes in PIEZO1** *Nature* **573**:230–234 Google Scholar

12. Cox C. D., et al. (2016) **Removal of the mechanoprotective influence of the cytoskeleton reveals PIEZO1 is gated by bilayer tension** *Nature communications* **7**:1–13 Google Scholar

13. Lewis A. H., Grandl J. (2015) **Mechanical sensitivity of Piezo1 ion channels can be tuned by cellular membrane tension** *Elife* **4**:e12088 Google Scholar

14. Haselwandter C. A., MacKinnon R. (2018) **Piezo's membrane footprint and its contribution to mechanosensitivity** *Elife* **7**:e41968 Google Scholar

15. Bavi N., Richardson J., Heu C., Martinac B., Poole K. (2019) **PIEZO1-mediated currents are modulated by substrate mechanics** *ACS nano* **13**:13545–13559 Google Scholar

16. Wang J., et al. (2022) **Tethering Piezo channels to the actin cytoskeleton for mechanogating via the cadherin-β-catenin mechanotransduction complex** *Cell Reports*

38:110342 Google Scholar

17. Verkest C., et al. (2022) **Intrinsically disordered intracellular domains control key features of the mechanically-gated ion channel PIEZO2** *Nature Communications* **13**:1–14 Google Scholar

18. Romero L. O., et al. (2020) **A dietary fatty acid counteracts neuronal mechanical sensitization** *Nature communications* **11**:1–12 Google Scholar

19. Vaisey G., Banerjee P., North A. J., Haselwandter C. A., MacKinnon R. (2022) **Piezo1 as a force-through-membrane sensor in red blood cells** *bioRxiv* Google Scholar

20. Mylvaganam S., et al. (2022) **The spectrin cytoskeleton integrates endothelial mechanoresponses** *Nat. Cell Biol* **24**:1226–1238 Google Scholar

21. Dumitru A. C., et al. (2021) **Probing PIEZO1 Localization upon Activation Using High-Resolution Atomic Force and Confocal Microscopy** *Nano Letters* **21**:4950–4958 Google Scholar

22. Pathak M. M., et al. (2014) **Stretch-activated ion channel Piezo1 directs lineage choice in human neural stem cells** *Proceedings of the National Academy of Sciences* **111**:16148–16153 Google Scholar

23. Shi Z., Graber Z. T., Baumgart T., Stone H. A., Cohen A. E. (2018) **Cell membranes resist flow** *Cell* **175**:1769–1779 Google Scholar

24. Cohen A. E., Shi Z. (2020) **Do Cell Membranes Flow Like Honey or Jiggle Like Jello?** *Bioessays* **42**:1900142 Google Scholar

25. Ellefsen K. L., et al. (2019) **Myosin-II mediated traction forces evoke localized Piezo1-dependent Ca 2 flickers** *Communications biology* **2**:1–13 Google Scholar

26. Cohen A. E., Sarah Innes-Gold, Shi Z. (2022) **Membrane tension propagation couples axon growth and collateral branching** *Sci. Adv* **8**:eabo1297 Google Scholar

27. Yao M., et al. (2020) **Force-dependent Piezo1 recruitment to focal adhesions regulates adhesion maturation and turnover specifically in non-transformed cells** *bioRxiv* Google Scholar

28. Holt J. R., et al. (2021) **Spatiotemporal dynamics of PIEZO1 localization controls keratinocyte migration during wound healing** *Elife* **10**:e65415 Google Scholar

29. Chen X., et al. (2018) **A feedforward mechanism mediated by mechanosensitive ion channel PIEZO1 and tissue mechanics promotes glioma aggression** *Neuron* **100**:799–815 Google Scholar

30. Jiang F., et al. (2021) **The mechanosensitive Piezo1 channel mediates heart mechano-chemo transduction** *Nature communications* **12**:1–14 Google Scholar

31. Yu Z., et al. (2022) **Piezo1 is the cardiac mechanosensor that initiates the cardiomyocyte hypertrophic response to pressure overload in adult mice** *Nature Cardiovascular Research* **1**:577–591 Google Scholar

32.	Carrillo-Garcia J., et al. (2021) **The mechanosensitive Piezo1 channel controls endosome trafficking for an efficient cytokinetic abscission** *Science advances* **7**:eabi7785 Google Scholar

33.	Efremov A. K., et al. (2022) **Application of piconewton forces to individual filopodia reveals mechanosensory role of L-type Ca2 channels** *Biomaterials* :121477 Google Scholar

34.	Rosholm K. R., et al. (2017) **Membrane curvature regulates ligand-specific membrane sorting of GPCRs in living cells** *Nature chemical biology* **13**:724–729 Google Scholar

35.	Lou H., et al. (2019) **Membrane curvature underlies actin reorganization in response to nanoscale surface topography** *Proceedings of the National Academy of Sciences* **116**:23143–23151 Google Scholar

36.	Zhao W., et al. (2017) **Nanoscale manipulation of membrane curvature for probing endocytosis in live cells** *Nature nanotechnology* **12**:750–756 Google Scholar

37.	Syeda R., et al. (2015) **Chemical activation of the mechanotransduction channel Piezo1** *Elife* **4**:e07369 Google Scholar

38.	Lauritzen I., et al. (2005) **Cross-talk between the mechano-gated K2P channel TREK-1 and the actin cytoskeleton** *EMBO Rep* **6**:642–648 Google Scholar

39.	Baumgart T., Capraro B. R., Zhu C., Das S. L. (2011) **Thermodynamics and mechanics of membrane curvature generation and sensing by proteins and lipids** *Annu. Rev. Phys. Chem* **62**:483 Google Scholar

40.	Shi Z., Baumgart T. (2015) **Membrane tension and peripheral protein density mediate membrane shape transitions** *Nature communications* **6**:1–8 Google Scholar

41.	Mattila P. K., Lappalainen P. (2008) **Filopodia: molecular architecture and cellular functions** *Nature reviews Molecular cell biology* **9**:446–454 Google Scholar

42.	Charras G. T., Yarrow J. C., Horton M. A., Mahadevan L., Mitchison T. J. (2005) **Non-equilibration of hydrostatic pressure in blebbing cells** *Nature* **435**:365–369 Google Scholar

43.	Derényi I., Jülicher F., Prost J. (2002) **Formation and interaction of membrane tubes** *Phys. Rev. Lett* **88**:238101 Google Scholar

44.	Haselwandter C. A., MacKinnon R., Guo Y., Fu Z. (2022) **Quantitative prediction and measurement of Piezo's membrane footprint** *bioRxiv* Google Scholar

45.	Prévost C., et al. (2015) **IRSp53 senses negative membrane curvature and phase separates along membrane tubules** *Nature communications* **6**:1–11 Google Scholar

46.	Deserno M. (2007) **Fluid lipid membranes–a primer** http://www.cmu.edu/biolphys/deserno/pdf/membrane_theory.pdf

47.	Su M., et al. (2020) **Comparative study of curvature sensing mediated by f-bar and an intrinsically disordered region of fbp17** *Iscience* **23**:101712 Google Scholar

48.	De Vecchis D., Beech D. J., Kalli A. C. (2021) **Molecular dynamics simulations of Piezo1 channel opening by increases in membrane tension** *Biophys. J* **120**:1510–1521 Google Scholar

49. Jiang W., et al. (2021) **Crowding-induced opening of the mechanosensitive Piezo1 channel in silico** *Communications Biology* **4**:1–14 Google Scholar

50. Sorre B., et al. (2012) **Nature of curvature coupling of amphiphysin with membranes depends on its bound density** *Proceedings of the National Academy of Sciences* **109**:173–178 Google Scholar

51. Zhu C., Das S. L., Baumgart T. (2012) **Nonlinear sorting, curvature generation, and crowding of endophilin N-BAR on tubular membranes** *Biophys. J* **102**:1837–1845 Google Scholar

52. Lewis A. H., Grandl J. (2021) **Piezo1 ion channels inherently function as independent mechanotransducers** *Elife* **10**:e70988 Google Scholar

53. Ridone P., et al. (2020) **Disruption of membrane cholesterol organization impairs the activity of PIEZO1 channel clusters** *J. Gen. Physiol* **152** Google Scholar

54. Kabaso D., et al. (2012) **On the role of membrane anisotropy and BAR proteins in the stability of tubular membrane structures** *J. Biomech* **45**:231–238 Google Scholar

55. Alimohamadi H., Bell M. K., Halpain S., Rangamani P. (2021) **Mechanical principles governing the shapes of dendritic spines** *Frontiers in Physiology* :836 Google Scholar

56. Syeda R., et al. (2016) **Piezo1 channels are inherently mechanosensitive** *Cell reports* **17**:1739–1746 Google Scholar

57. Xie Q., et al. (2022) **Transcription factor Acj6 controls dendrite targeting via a combinatorial cellsurface code** *Neuron* Google Scholar

58. Song Y., et al. (2019) **The mechanosensitive ion channel piezo inhibits axon regeneration** *Neuron* **102**:373–389 Google Scholar

59. Ma N., et al. (2022) **Piezo1 regulates the regenerative capacity of skeletal muscles via orchestration of stem cell morphological states** *Science advances* **8**:eabn0485 Google Scholar

60. Ranade S. S., et al. (2014) **Piezo1, a mechanically activated ion channel, is required for vascular development in mice** *Proceedings of the National Academy of Sciences* **111**:10347–10352 Google Scholar

61. Nilufar S., Morrow A. A., Lee J. M., Perkins T. J. (2013) **FiloDetect: automatic detection of filopodia from fluorescence microscopy images** *BMC systems biology* **7**:1–12 Google Scholar

62. Wang H., Kelley F. M., Milovanovic D., Schuster B. S., Shi Z. (2021) **Surface tension and viscosity of protein condensates quantified by micropipette aspiration** *Biophysical Reports* :100011 Google Scholar

63. Stachowiak J. C., et al. (2012) **Membrane bending by protein–protein crowding** *Nat. Cell Biol* **14**:944–949 Google Scholar

64. Kang M., Day C. A., Kenworthy A. K., DiBenedetto E. (2012) **Simplified equation to extract diffusion coefficients from confocal FRAP data** *Traffic* **13**:1589–1600 Google Scholar

65. Helfrich W. (1973) **Elastic properties of lipid bilayers: theory and possible experiments** *Zeitschrift für Naturforschung c* **28**:693–703 Google Scholar

66. Haselwandter C. A., Guo Y., Fu Z., MacKinnon R. (2022) **Elastic properties and shape of the Piezo dome underlying its mechanosensory function** *bioRxiv*   Google Scholar

Author information

Shilong Yang

Department of Chemistry and Chemical Biology, Piscataway, NJ 08854, United States
ORCID iD: 0000-0002-4276-8646

Xinwen Miao[#]

School of Chemistry, Chemical Engineering, and Biotechnology, Nanyang Technological University, 637457, Singapore

[#]X.M., S.A., and B.L. contributed equally to this study.

Steven Arnold[#]

Department of Cell Biology and Neuroscience, Piscataway, NJ 08854, United States

[#]X.M., S.A., and B.L. contributed equally to this study.

Boxuan Li[#]

Department of Chemistry and Chemical Biology, Piscataway, NJ 08854, United States

[#]X.M., S.A., and B.L. contributed equally to this study.

Alan T. Ly

Department of Physiology & Biophysics, UC Irvine, CA 92697, United States, Sue and Bill Gross Stem Cell Research Center

Huan Wang

Department of Chemistry and Chemical Biology, Piscataway, NJ 08854, United States

Matthew Wang

Department of Physics, Rutgers University, Piscataway, NJ 08854, United States

Xiangfu Guo

School of Chemistry, Chemical Engineering, and Biotechnology, Nanyang Technological University, 637457, Singapore

Medha M. Pathak

Department of Physiology & Biophysics, UC Irvine, CA 92697, United States, Sue and Bill Gross Stem Cell Research Center

Wenting Zhao

School of Chemistry, Chemical Engineering, and Biotechnology, Nanyang Technological University, 637457, Singapore

Charles D. Cox

Molecular Cardiology and Biophysics Division, Victor Chang Cardiac Research Institute, Sydney, NSW, Australia
ORCID iD: 0000-0002-3802-6746

Zheng Shi

Department of Chemistry and Chemical Biology, Piscataway, NJ 08854, United States, Cancer Pharmacology Research Program, Cancer Institute of New Jersey, Rutgers University, New Brunswick, NJ 08901, United States
ORCID iD: 0000-0002-5214-1871

Correspondence should be addressed to: zheng.shi@rutgers.edu

Copyright

Authors' response (5 November 2022)

> *GENERAL ASSESSMENT*
>
> *Piezo1 and Piezo2 are stretch-gated ion channels that are critically important in a wide range of physiological processes, including vascular development, touch sensation and wound repair. These remarkably large molecules span the plasma membrane almost 40 times. Cryo-EM and reconstitution experiments have shown that Piezos adopt a cup-like structure and, by doing so, curve the local membrane in which they are embedded. Importantly, membrane tension is a key mediator of Piezo function and gating, an idea well-supported several independent studies. Cells have varied three-dimensional shapes and are dynamic assemblies surrounded by plasma membranes with complex topologies and biochemical landscapes. How these microenvironments influence mechanosensation and Piezo function are unknown.*
>
> *The current preprint by Zheng Shi and colleagues asks how the shape of the membrane influences Piezo location. The authors use creative approach involving methods to distort the plasma membrane by generating "blebs" and artificial "filopodia". Overall, the work convincingly shows that the curvature of the lipid environment influences Piezo localization. Specifically, they show that Piezo1 molecules are excluded from filopodia and other highly curved membranes. These experiments are well controlled and the results fully consistent with previous structural and biochemical work. Furthermore, the work explores the hypothesis that a chemical modulator of Piezo1 channels called Yoda1 functions by "flattening" the channels, a movement previously proposed to be linked to mechanical gating. Consistent with this model, the authors show that Yoda1 application is sufficient to allow Piezo1 channels to enter filopodia. While the flattening model is provocative hypothesis, hard evidence awaits structural verification.*
>
> *Overall, the preprint by Shi and colleagues will be of interest to scientists studying how mechanical forces are detected at the molecular level. The work introduces important concepts regarding how the shape of cellular membranes affects the movement and*

function of proteins within it. The technical advance for changing the shape of a plasma membrane is of note.

We thank the reviewers for the accurate summary and positive assessments of our manuscript. We address each of the concerns below.

> **RECOMMENDATIONS**
>
> **Revisions essential for endorsement:**
>
> *As is evident from the comments below, our endorsement of the study is not dependent on additional experiments. However, we feel more experimental clarification is needed, that providing clearer images would be helpful, and, most importantly, we would like alternative conclusions and caveats to be mentioned.*
>
> *1. Can the authors comment on the link between the conclusions that (1) the presence of filopodia prohibits Piezo1 localization (Fig 1) and (2) Piezo1 expression prohibits the formation of filopodia (Fig 3). As it stands, it is hard to understand if there is a cause and effect relationship here or if these are separate, unrelated observations? We recommend revising the discussion to clarify.*

We now clarify the link between Piezo1's curvature sensing (depletion from filopodia) and its inhibition effect on filopodia formation before presenting the current Fig. 5: "Curvature sensing proteins often have a modulating effect on membrane geometry. For example, N-BAR proteins, which strongly enrich to positive membrane curvature, can mechanically promote endocytosis by making it easier to form membrane invaginations (Shi and Baumgart, 2015; Sorre et al., 2012). Thus, we hypothesize that Piezo1, which strongly depletes from negative membrane curvature (Fig. 1, Fig. 2), can have an inhibitory effect on the formation of membrane protrusions such as filopodia."

> *2. When comparing the images of Fig. 2A, B to those of Fig. 2C, D, it appears that bleb formation induces a drastic enrichment of Piezo1 in the bleb membrane. Is this due to low membrane tension in the bleb? If this is the case, it indicates that the level of membrane tension has a prominent role in determining the localization of Piezo1.*

We apologize for this confusion due to our poor wording and figure presentation in the manuscript. By "Piezo1 clearly locates to bleb membranes" we didn't mean to indicate that Piezo1 is enriched on bleb membranes as compared to the cell body. Rather, we meant to emphasize Piezo1's localization to the *membrane* of the blebs rather than in the cytosolic space.

Cells in 2C, 2D are different from that in 2A and 2B and were presented with different image contrasts. We now include the images of the full cell for Fig. 2C and 2D as the current Figure S8. To focus on the equator of the bleb, the cell body was out of focus. However, there is no indication that Piezo1 density is significantly different between the bleb membrane and the intact parts of the plasma membrane.

We changed the main text to: "Similar to previous reports (Cox et al., 2016), bleb membranes clearly contain Piezo1 signal, but not significantly enriched relative to the cell body (Fig. 2C, 2D; Fig. S8)."

> *In line with this, it appears more Piezo1 proteins are localized in less tensed tethers. Thus, might your observations be equally consistent with tension rather than curvature as a key regulator of Piezo1 localization? We recommend adding this to your discussion.*

We now explain the deconvolution between tension and curvature effects in detail. We also performed additional experiments to quantify the membrane tension in cells and blebs (current Fig. S9).

In the Results section, we add: "Tethers are typically imaged > 1 min after pulling, whereas membrane tension equilibrates within 1 s across cellular scale free membranes (e.g., bleb, tether) (Shi et al., 2018). Therefore, the sorting of Piezo1 within individual tension-equilibrated tether-bleb systems (Fig. 2C – 2G) suggests that membrane curvature can directly modulate Piezo1 distribution beyond potential confounding tension effects."

In the Discussion section, we add: "In addition to membrane curvature, tension in the membrane may affect the subcellular distribution of Piezo1 (Dumitru et al., 2021). Particularly, membrane tension can activate the channel and potentially change Piezo1's nano-geometries. This tension effect is unlikely to play a significant role in our interpretation of the curvature sorting of Piezo1 (Fig .2): (1) HeLa cell membrane tension as probed by short tethers (Fig. S9F; 45 ± 29 pN/ μm on blebs and 270 ± 29 pN/ μm on cells, with the highest recorded tension at 426 pN/ μm) are significantly lower than the activation tension for Piezo1 (> 1000 pN/μm (Cox et al., 2016; Lewis and Grandl, 2015; Shi et al., 2018; Syeda et al., 2016)). (2) With more activated (and potentially flatten) channels under high membrane tension, one would expect a higher density of Piezo1 on tethers pulled from tenser blebs. This is the opposite to our observations in Fig. 2C - 2G, where Piezo1 density on tethers was found to decrease with the absolute curvature, thus tension (eq. S6), of membrane tethers."

> *3. Given the intrinsically curved structure of Piezo1, it is difficult to understand the model's prediction that curved Piezo1 is not enriched in 25-75 nm invaginations. Where will Piezo1 normally reside in the plasma membrane? It would be helpful if this could be discussed.*

The spontaneous curvature from our model C_0 (C_0-1 = 83 ± 17 nm, the value is updated after refitting to more data points collected for Fig. 2G) represents a balance between the intrinsic curvature of Piezo1 trimers (0.04 ~ 0.2 nm-1 as suggested by CryoEM studies(Haselwandter et al., 2022; Lin et al., 2019; Yang et al., 2022)) and that of the associated membrane (0 nm-1, assuming lipid bilayers alone do not have an intrinsic curvature). We now refer to C_0 as the "spontaneous curvature of the Piezo1-membrane complex" throughout the manuscript, rather than the "spontaneous curvature of Piezo1".

Our model, when extrapolated to membrane invaginations, predicts a weak enrichment of Piezo1 on ~100 nm invaginations (peak at 83 nm), but a depletion of Piezo1 on more highly curved invaginations. This is simply because it would be energetically costly to fit a protein-membrane complex to a curvature that is different from what the complex prefers (in the case of 25-75 nm membrane invaginations, the membrane curvature would be too high for the Piezo1-memrbane complex).

However, it is worth pointing out that Piezo1-membrane complex may not present the same spontaneous curvature on positively and negatively curved membranes. More importantly, we do not yet have direct evidence to show that this depletion indeed happens in the exact range of invagination curvature we predicted. We now acknowledge this limitation in the Discussion section: "However, it is worth noting that we assumed a zero spontaneous curvature for membranes associated with Piezo1 and that the spontaneous curvature of Piezo1-membrane complex is independent of the shape of surrounding membranes. These assumptions may no longer hold when studying Piezo1 in highly curved invaginations or liposomes (Lin et al., 2019)."

We also took this opportunity to verify the key prediction from the extrapolated model - that Piezo1 would enrich towards ~ 100 nm radius cell membrane invaginations. To achieve this,

we utilized a recent development in nanotechnology, pioneered by Wenting Zhao and Bianxiao Cui's labs (Lou et al., 2019; Zhao et al., 2017). An illustration of the experimental design and detailed findings are summarized in the current Fig. 3 and briefly discussed below.

In collaboration with Wenting Zhao's lab, we cultured cells on precisely engineered nanobars with curved ends and flat central regions. For a labelled membrane protein of interest, the end-to-center fluorescence ratio would report the protein's curvature sorting ability. We find that Piezo1 enriches to the curved ends of nanobars, whereas membrane marker signals are homogeneous across the entire nanobar (Fig. 3). The finding achieved strong statistical significance via hundreds of repeats on nanobars of the exact same geometry, a major technical strength of our chosen system. Furthermore, the enrichment of Piezo1 was observed on nanobars with 3 different curvatures (corresponding to diffraction-limited radii between 100 to 200 nm) and qualitatively agrees with our model (current Fig. S10). While further investigations on a wider range of membrane curvature are required to fully map out the sorting of Piezo1 on membrane invaginations, our data in the current Fig. 3 clearly verifies the prediction that membrane curvature can lead to enrichment of Piezo1 on cellular invaginations.

We now refer to this new finding in the Abstract, along with the previously observed depletion of Piezo1 on filopodia. We present a detailed description of the experiment and associated findings in the Results and the Method sections.

> *4. It is currently unknown whether and how long Yoda1 might keep Piezo1 in a flattened state. Given that Yoda1 is highly hydrophobic, it might affect membrane properties instead of the curvature of Piezo1. These caveats should be discussed.*

We thank the reviewers for pointing out the potential effect of Yoda1. We did additional experiments to confirm that on Piezo1-KO cells, Yoda1 molecules alone do not significantly alter the formation of filopodia, in contrast to observations in WT cells. This data suggests Yoda1 (at the concentration we use) is unlikely to significantly alter the mechanical properties of the plasma membrane. The data is now presented as Fig. 5E in the updated manuscript. We added: "In Piezo1 knockout (Piezo1-KO) cells, adding Yoda1 to the culture medium does not significantly change the number of filopodia (Fig. 5E), suggesting the agonist does not directly regulate filopodia formation without acting on Piezo1."

> *5. The authors state that "Yoda1 leads to a Ca2+ independent increase of Piezo1 on tethers". It has not been determined yet that Yoda1 leads to Piezo1 flattening (or even opening). In Electrophysiology experiments, unless there is pressure applied, Yoda1 does not lead to substantial currents. Therefore, the cartoon of Yoda1 flattening Piezo1(3H) is misleading. We recommend revising this. So far, the best experimental evidence on flattening is via purified channels reconstituted in various sizes of liposomes. However, it is plausible that the flattened shape is closed or open inactivated. Because most of the claims of this paper depend on the curved vs flattened shape of Piezo1, the authors should address these caveats carefully.*

We thank the reviewers for pointing out the limitations in our current understanding of Yoda1. We agree that our data do not directly show the flattening of Piezo1 by Yoda1, rather it is consistent with the flattening hypotheses. We lowered the tone of our conclusion to Fig. 4 to: "Our study suggests this conformational change of Piezo1 may also happen in live cells (Fig. 4H)." We also added arrows in Fig. 4H to suggest that membrane tension helps the proposed flattening of Piezo1 by Yoda1.

We think our experiment may also provide new insights on the action of Yoda1: First, we note that only a small fraction of filopodia responded to Yoda1, and pre-stressing of the cell

membrane was required to amplify the Yoda1 effect (current Fig. 4E). This observation is consistent with the reviewers' notion that membrane tension is likely required to flatten Piezo1, even in the presence of Yoda1. Secondly, highly curved liposome or detergents can confine the shape of Piezo1 trimers. Therefore, the inability to observe Yoda1-induced flattening of Piezo1 in small liposomes is not necessarily in contradiction with our observation in the mostly flat cell membranes.

We add to the Discussion section: "Yoda1 induced flattening of Piezo1 has not been directly observed via CryoEM. Our results (Fig. 4) point to two challenges in determining this potential structural change: (1) Yoda1 induced changes in Piezo1 sorting is greatly amplified after pre-stretching the membrane (Fig. 4E), pointing to the possibility that a significant tension in the membrane is required for the flattening of Yoda1-bound Piezo1. (2) Piezo1 is often incorporated in small (< 20 nm radius) liposomes for CryoEM studies. The shape of liposomes can confine the nano-geometry of Piezo1 (Lin et al., 2019; Yang et al., 2022), rendering it significantly more challenging to respond to potential Yoda1 effects. This potential effect of membrane curvature on the activation of Piezo1 would be an interesting direction for future studies."

> *6. Page 9: "Our study shows this conformational change of Piezo1 in live cells (Fig. 3H)."*
> *We recommend that this claim be removed as it seems too strong for the provided data.*

We changed the sentence to: "Our study suggests this conformational change of Piezo1 may also happen in live cells (Fig. 4H)."

> **Additional suggestions for the authors to consider:**
>
> *1. Based on the calculated spontaneous curvature of Piezo1-membrane C0 of 87 nm, is it possible to derive the curvature of Piezo1 protein itself and the associated membrane footprint? This would be a nice addition.*

It is possible to do such an estimation, however, many (unverified) assumptions must be made, in addition to the ones already in our model. First, we need to assume a size of the Piezo1 trimers and of the Piezo1-membrane complex. If we assume Piezo1 trimers are ~170 nm2 in the plane of lipid bilayers (based on estimates from PDB) and that the complex takes on the shape of a 10 -20 nm radius half-sphere. Effectively, Piezo1 occupies an area fraction of 6.7%~27% in the Piezo1-membrane complex. Next, we assume that the membrane and the Piezo1 trimer have the same bending rigidity. Finally, we assume that the membrane itself does not have an intrinsic curvature.

With those assumptions, the intrinsic curvature of Piezo1 trimers (_C_p) would relate to the spontaneous curvature of membrane-Piezo1 complex (_C_0) following: _C_p-1 = _C_0-1 * (6.7%~27%). Knowing _C_0-1 = 83 ± 17 nm, we get _C_p-1 = 5.6 nm ~ 22.4 nm.

> *2. It is hard to see the filopodia and their localization in the figures. It would be better for readers and more convincing if clearer/higher resolution example images could be provided.*

We now provide high resolution figures.

> *3. Can the authors better explain how the calculations done in panel 1C and S3D are done and their importance?*

Each fluorescence trace along the drawn yellow line was normalized to the mean intensity on the corresponding flat cell body, so that the average fluorescence of the cell body has a y-axis value of 1. We think the intensity traces are important because image contrast can be

adjusted, therefore Fig. 1A alone would not convincingly show that there are no Piezo1 on filopodia.

> *4. In Figure 2E, are these data from hPiezo1 or mPiezo1? In other cases, hPiezo1 is specified, this this may be a typo?*

Corrected.

> *5. Figure 3 F&G: We assume these cells are the same in all panels, just visualized with either mCherry or eGFP in each condition. Accordingly, we would have expected more swelling in hypotonic conditions, and wonder if further evaluation may resolve this apparent discrepancy? If not, please provide more clarification.*

This is a good point. Indeed, we do observe a significant swelling of the cell right after the hypotonic shock.

However, this effect is expected to be transient (volume of the cell would recover after ~ 1 min), see Figure. 1C here: https://www.pnas.org/doi/10.1073/pnas.2103228118. Our images in Fig. 3F and 3G were taken ~10 min after the hypotonic shock.

> *6. On a lighter note, we'd recommend not using in cellulo.*

We changed in cellulo to "in live cells"

Reference List

Cox, C.D., Bae, C., Ziegler, L., Hartley, S., Nikolova-Krstevski, V., Rohde, P.R., Ng, C., Sachs, F., Gottlieb, P.A., and Martinac, B. (2016). Removal of the mechanoprotective influence of the cytoskeleton reveals PIEZO1 is gated by bilayer tension. Nature Communications *7*, 1-13.

Dumitru, A.C., Stommen, A., Koehler, M., Cloos, A., Yang, J., Leclercqz, A., Tyteca, D., and Alsteens, D. (2021). Probing PIEZO1 Localization upon Activation Using High-Resolution Atomic Force and Confocal Microscopy. Nano Letters *21*, 4950-4958.

Haselwandter, C.A., MacKinnon, R., Guo, Y., and Fu, Z. (2022). Quantitative prediction and measurement of Piezo's membrane footprint. bioRxiv

Lewis, A.H., and Grandl, J. (2015). Mechanical sensitivity of Piezo1 ion channels can be tuned by cellular membrane tension. Elife *4*, e12088.

Lin, Y., Guo, Y.R., Miyagi, A., Levring, J., MacKinnon, R., and Scheuring, S. (2019). Force-induced conformational changes in PIEZO1. Nature *573*, 230-234.

Lou, H., Zhao, W., Li, X., Duan, L., Powers, A., Akamatsu, M., Santoro, F., McGuire, A.F., Cui, Y., and Drubin, D.G. (2019). Membrane curvature underlies actin reorganization in response to nanoscale surface topography. Proceedings of the National Academy of Sciences *116*, 23143-23151.

Shi, Z., and Baumgart, T. (2015). Membrane tension and peripheral protein density mediate membrane shape transitions. Nature Communications *6*, 1-8.

Shi, Z., Graber, Z.T., Baumgart, T., Stone, H.A., and Cohen, A.E. (2018). Cell membranes resist flow. Cell *175*, 1769-1779. e13.

Sorre, B., Callan-Jones, A., Manzi, J., Goud, B., Prost, J., Bassereau, P., and Roux, A. (2012). Nature of curvature coupling of amphiphysin with membranes depends on its bound density. Proceedings of the National Academy of Sciences *109*, 173-178.

Syeda, R., Florendo, M.N., Cox, C.D., Kefauver, J.M., Santos, J.S., Martinac, B., and Patapoutian, A. (2016). Piezo1 channels are inherently mechanosensitive. Cell Reports *17,* 1739-1746.

Yang, X., Lin, C., Chen, X., Li, S., Li, X., and Xiao, B. (2022). Structure deformation and curvature sensing of PIEZO1 in lipid membranes. Nature 1-7.

Zhao, W., Hanson, L., Lou, H., Akamatsu, M., Chowdary, P.D., Santoro, F., Marks, J.R., Grassart, A., Drubin, D.G., and Cui, Y. (2017). Nanoscale manipulation of membrane curvature for probing endocytosis in live cells. Nature Nanotechnology *12,* 750-756.

(This is a response to peer review conducted by Biophysics Colab on version 1 of this preprint.)